

ARTICLE

# $\alpha$ -Catenin links integrin adhesions to F-actin to regulate ECM mechanosensing and rigidity dependence

Abhishek Mukherjee<sup>1</sup>, Shay Melamed<sup>1</sup>, Hana Damouny-Khoury<sup>1</sup>, Malak Amer<sup>1</sup>, Lea Feld<sup>1</sup>, Elisabeth Nadjar-Boger<sup>1</sup>, Michael P. Sheetz<sup>2</sup>, and Haguy Wolfenson<sup>1</sup>

**Both cell-cell and cell-matrix adhesions are regulated by mechanical signals, but the mechanobiological processes that mediate the cross talk between these structures are poorly understood. Here we show that  $\alpha$ -catenin, a mechanosensitive protein that is classically linked with cadherin-based adhesions, associates with and regulates integrin adhesions.  $\alpha$ -Catenin is recruited to the edges of mesenchymal cells, where it interacts with F-actin. This is followed by mutual retrograde flow of  $\alpha$ -catenin and F-actin from the cell edge, during which  $\alpha$ -catenin interacts with vinculin within integrin adhesions. This interaction affects adhesion maturation, stress-fiber assembly, and force transmission to the matrix. In epithelial cells,  $\alpha$ -catenin is present in cell-cell adhesions and absent from cell-matrix adhesions. However, when these cells undergo epithelial-to-mesenchymal transition,  $\alpha$ -catenin transitions to the cell edge, where it facilitates proper mechanosensing. This is highlighted by the ability of  $\alpha$ -catenin-depleted cells to grow on soft matrices. These results suggest a dual role of  $\alpha$ -catenin in mechanosensing, through both cell-cell and cell-matrix adhesions.**

## Introduction

The ability of cells to sense and respond to their immediate environment affects the most fundamental cellular functions, including as survival, proliferation, and migration (Ringer et al., 2017; Iskratsch et al., 2014; Yap et al., 2018). This sensing ability relies on direct physical interactions with neighboring cells or with the ECM through cell adhesion molecules—cadherins and integrins, respectively (Maiden and Hardin, 2011). The balance and transition between these two types of interactions can determine the state of a cell, as in the process of epithelial-to-mesenchymal transition (EMT). However, the mechanisms of interplay between cell-cell and cell-matrix adhesions remain poorly understood.

Cell-cell contacts are classically mediated by adherens junctions (AJs), which are composed of transmembrane E-cadherin molecules and the catenin family of proteins—p120-catenin,  $\beta$ -catenin, and  $\alpha$ -catenin—that bind as a complex to the cytoplasmic tails of the cadherins (Pokutta and Weis, 2007).  $\alpha$ -Catenin is an actin-binding protein, and its ability to mediate the connection between cadherin and F-actin is vital for AJs, as actomyosin-based forces are required for stabilizing the cadherin-cadherin connection (Sarpal et al., 2019; Yonemura

et al., 2010). In this process,  $\alpha$ -catenin acts as a mechanosensory protein that responds to the applied forces in the form of structural changes that occur in its C-terminal actin-binding domain (ABD) and in its M-domain (Barry et al., 2014; Buckley et al., 2014; Thomas et al., 2013). The M-domain recruits numerous adhesion-related proteins, including ZO-1, afadin,  $\alpha$ -actinin, and vinculin (Kobielak and Fuchs, 2004). Notably, the latter two are also important mediators of the connection between integrins and F-actin within focal adhesions (FAs; Parsons et al., 2010; Wolfenson et al., 2013), suggesting a possible involvement of  $\alpha$ -catenin in these structures. Previous studies have suggested a role for  $\alpha$ -catenin outside of cell-cell adhesions (Sun et al., 2014; Vassilev et al., 2017; Wood et al., 2017; Piao et al., 2014), but whether  $\alpha$ -catenin plays a role in regulating cell-matrix adhesions and ECM mechanosensing is unknown.

Here we show that in mesenchymal cells,  $\alpha$ -catenin is recruited to the cell edge, where it interacts with F-actin in regions devoid of  $\alpha$ -actinin. It then undergoes retrograde flow together with F-actin toward the cell center and interacts with vinculin within integrin adhesions. This interaction mediates adhesion maturation, enhances force transmission to the matrix, and

<sup>1</sup>Department of Genetics and Developmental Biology, Rappaport Faculty of Medicine, Technion—Israel Institute of Technology, Haifa, Israel; <sup>2</sup>Department of Biochemistry and Molecular Biology, University of Texas Medical Branch, Galveston, TX.

Correspondence to Haguy Wolfenson: [haguyw@technion.ac.il](mailto:haguyw@technion.ac.il).

© 2022 Mukherjee et al. This article is distributed under the terms of an Attribution–Noncommercial–Share Alike–No Mirror Sites license for the first six months after the publication date (see <http://www.rupress.org/terms/>). After six months it is available under a Creative Commons License (Attribution–Noncommercial–Share Alike 4.0 International license, as described at <https://creativecommons.org/licenses/by-nc-sa/4.0/>).



drives the proper assembly of actin stress fibers. We find that while the loss of  $\alpha$ -catenin is not sufficient to induce EMT on its own, it does play a role in rigidity-dependent EMT induced by TGF $\beta$ . Importantly, after EMT,  $\alpha$ -catenin transitions to the edges of the cells, where it facilitates mechanosensing. Moreover, the absence of the  $\alpha$ -catenin–vinculin interaction causes mesenchymal cells to display impaired adhesion to the matrix. This results in aberrant mechanosensing of the matrix and the transformation of cells to being rigidity independent for growth.

## Results and discussion

### $\alpha$ -Catenin localizes to the edges of fibroblast cells

Since  $\alpha$ -catenin was shown to be recruited to mesenchymal cell edges (Wood et al., 2017), we postulated that it might play a role in regulating integrin adhesions that assemble in those regions. To test this, we first verified the recruitment of  $\alpha$ -catenin to the cell edges of three different fibroblast cell lines: RPTP $\alpha^{+/+}$  mouse embryonic fibroblasts (MEFs), NIH3T3 cells, and human foreskin fibroblasts (HFFs). We plated the cells sparsely on fibronectin (FN)-coated coverslips to prevent the formation of cell–cell contacts and fixed them after 15 min of spreading. We confirmed by immunostaining that in 50–60% of these cells,  $\alpha$ -catenin was localized in lamellipodial regions (typically presented as narrow stripes at the cell edge;  $\sim$ 500 nm for MEF and NIH3T3,  $\sim$ 1,200 nm for HFF; Fig. 1 A).

Next, we set out to characterize the interaction of  $\alpha$ -catenin with its known binding partners in AJs—F-actin,  $\alpha$ -actinin, and vinculin—in mesenchymal cells, as they are all key players in integrin adhesions. To that end, we used the MEFs, which typically express high levels of the  $\alpha$ E-catenin isoform (Fig. S1 A). Notably, the recruitment of  $\alpha$ -catenin to the cell edge was independent of vinculin and  $\alpha$ -actinin, as their depletion from the cells did not affect  $\alpha$ -catenin localization (Fig. S1 B). Costaining the cells for  $\alpha$ -catenin and F-actin showed that they were often colocalized at the cell edge at early stages of cell spreading (Fig. 1 B). Closer examination of cell centers also revealed striped patterns of  $\alpha$ -catenin that coincided with actin stress fibers in the majority of analyzed cells (although these patterns were sometimes obscured by cytoplasmic staining; Figs. 1 B and S1 C). We then costained the cells for  $\alpha$ -catenin,  $\alpha$ -actinin, and F-actin. Consistent with previous studies, after 15 min of cell spreading,  $\alpha$ -actinin appeared in nascent adhesion sites and was also recruited to the cell edges, where it was colocalized with F-actin (Fig. S2 A; Meacci et al., 2016; Roca-Cusachs et al., 2013). However, closer examination of high-resolution confocal images showed that  $\alpha$ -catenin and  $\alpha$ -actinin were not colocalized at the cell edges (Fig. S2 B). Similarly, at later time points, these two proteins were not colocalized on actin stress fibers (Fig. S2 C). Thus,  $\alpha$ -actinin and  $\alpha$ -catenin overlaid actin filaments in a non-overlapping manner.

We next turned to test the relative distributions of  $\alpha$ -catenin and vinculin. In cells that displayed nascent vinculin adhesions at the cell edge, we found similar distributions of  $\alpha$ -catenin, although colocalization was partial (Fig. 1 C). Also, in some cells that displayed mature vinculin adhesions 1–3  $\mu$ m away from the  $\alpha$ -catenin–rich cell edges, we observed  $\alpha$ -catenin patches

extending from the edges toward these adhesions (Fig. 1 D), suggesting that  $\alpha$ -catenin was flowing from the cell edges toward integrin adhesions and interacting with them. This was observed in a relatively small number of cases, suggesting that such an interaction might be transient and would be better detected by live-cell imaging.

### $\alpha$ -Catenin undergoes retrograde flow with F-actin and interacts with integrin adhesions

To further explore the relationship of  $\alpha$ -catenin with F-actin, vinculin, and  $\alpha$ -actinin in the context of the lamellipodium and integrin adhesions, we performed live-cell imaging of MEFs on FN-coated coverslips. Tracking the dynamics of WT GFP- $\alpha$ -catenin along with the F-actin marker tdTomato-Tractin (Belin et al., 2014) showed that the two markers were predominantly colocalized and displayed the same protrusion–retraction cycles at the cell edge (Fig. 2, A and A'; and Video 1). Moreover, GFP- $\alpha$ -catenin displayed the same flow patterns as F-actin from the cell edge inwards and decorated actin stress fibers as they gradually grew over time (Video 1). Consistent with the immunostaining results, imaging of live cells coexpressing GFP- $\alpha$ -catenin and mCherry- $\alpha$ -actinin showed that they did not overlap (Video 2). In particular, during protrusion–retraction cycles, when  $\alpha$ -actinin was associated with the protrusion phase,  $\alpha$ -catenin was associated with the retraction phase, and vice versa (Fig. S2, D and D'). Thus,  $\alpha$ -catenin and  $\alpha$ -actinin do not interact within the context of cell edge dynamics and integrin adhesions.

In contrast, imaging of live cells coexpressing GFP- $\alpha$ -catenin and mCherry-vinculin showed that they had similar dynamics and flow patterns. In particular,  $\alpha$ -catenin colocalized with vinculin within adhesions that were growing and sliding from the cell edge toward the center (Fig. 2 B' and Video 3), suggesting a specific interaction between  $\alpha$ -catenin and maturing FAs. Indeed, temporal averaging of GFP- $\alpha$ -catenin videos revealed patterns of  $\alpha$ -catenin expression that matched the localization of FAs situated 1–3  $\mu$ m inwards from the cell edge (Fig. 2 B).

### $\alpha$ -Catenin interacts with vinculin in FAs

To further explore the interaction between  $\alpha$ -catenin and FAs, we next tested whether a specific connection between  $\alpha$ -catenin and vinculin was an underlying reason for their similar flow patterns. Indeed, coimmunoprecipitation (co-IP) showed a direct association between the two proteins, which was lost upon  $\alpha$ -catenin knockdown (KD) and restored upon expression of WT GFP- $\alpha$ -catenin (Fig. S3 A). We therefore used a variant of GFP- $\alpha$ -catenin containing a lysine-to-proline mutation at site 344 (L344P) that displays drastically diminished binding to vinculin (Peng et al., 2012; Seddiki et al., 2018). We expressed this variant, along with tdTomato-Tractin or mCherry-vinculin, in  $\alpha$ -catenin KD MEFs and performed live-cell tracking of the cells. This revealed stark differences in the  $\alpha$ -catenin and adhesion dynamics compared with those detected in WT GFP- $\alpha$ -catenin cells. First, in  $\sim$ 61% of the analyzed L344P mutant cells (14 of  $n = 23$  cells), stable adhesions failed to form, and as a result the cell edges did not stabilize following protrusions, leading to extensive ruffling (Fig. 3 A and Video 4). This was confirmed using

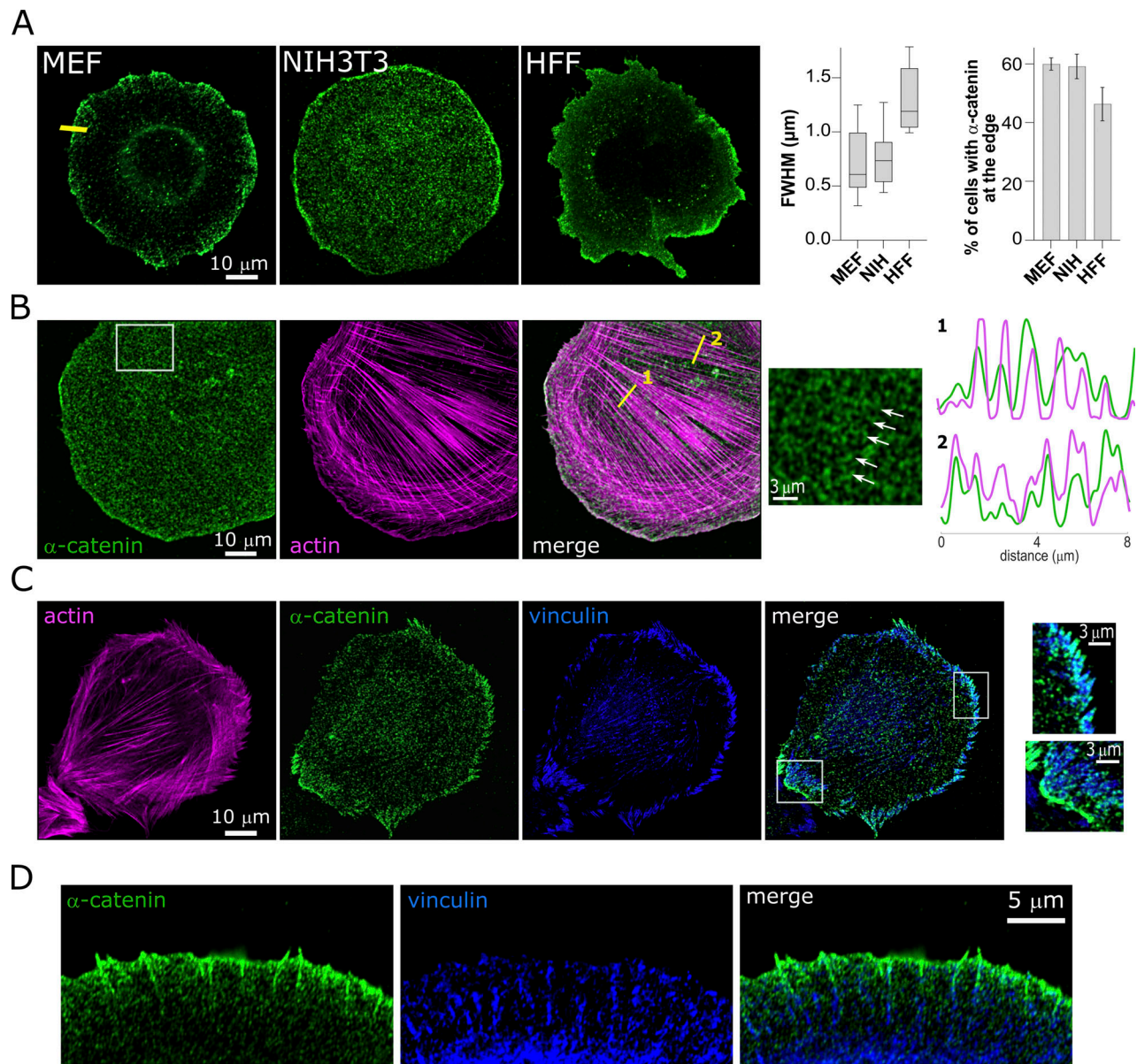


**Figure 1.  $\alpha$ -Catenin localizes in the lamellipodium at early times of cell spreading.** (A) Representative images of three fibroblast cell lines immunostained for  $\alpha$ -catenin after 15 min of spreading on FN-coated coverslips (left), along with the width of the catenin band at the cell edge, represented by full width half maximum (FWHM; center), and the percentage of cells from each fibroblast cell line with catenin at the cell-edge (right;  $n = 30$  cells in each case). (B) WT MEFs costained for  $\alpha$ -catenin and F-actin (phalloidin); the right panel is a zoom-in of the box in the left image, showing  $\alpha$ -catenin stripes that coincide with stress fibers; the graphs on the right are the normalized intensities of phalloidin (magenta) and  $\alpha$ -catenin (green) measured along the yellow lines in the merged image. (C) WT MEF costained for actin,  $\alpha$ -catenin, and vinculin; right panel images are zoom-ins of the boxes in the merged image, showing vinculin and  $\alpha$ -catenin in cell-matrix (top) and cell-cell (bottom) adhesions. (D) Zoom-in on the edge of a WT MEF cell costained for  $\alpha$ -catenin and vinculin.

live bright-field imaging of early cell spreading in which  $\alpha$ -catenin KD cells and L344P mutant cells displayed extensive ruffling compared with WT controls (Videos 5, 6, 7, and 8 and Fig. S3 B). Second, in  $\sim 26\%$  of the cells, the cell edges were able to stabilize without the formation of lamellipodia, and instead the cells spread by projecting narrow protrusions (Fig. 3 B). However, even though relatively stable vinculin-containing adhesions were present in such protrusions, these adhesions rarely slid toward the cell center, despite the observed retrograde flow of GFP- $\alpha$ -catenin-L344P on top of them (Fig. 3 B and Video 9). Rather, the GFP- $\alpha$ -catenin-L344P flow rate was considerably

higher than that of mCherry-vinculin in these adhesions ( $12.4 \pm 1.1$  vs.  $6.4 \pm 0.7$  nm/s;  $n = 20$  for each; Fig. 3 B and Video 9). Finally, at the cellular level, GFP- $\alpha$ -catenin-L344P was often located on actin stress fibers that were attached to vinculin adhesions, but unlike cells expressing WT GFP- $\alpha$ -catenin, the stress fibers were highly contractile and dynamic (Fig. 3, C and D; and Video 10). This led to the perturbation of the actin cytoskeleton organization, which was initially characterized by the aggregation of GFP- $\alpha$ -catenin-L344P along with F-actin at the cell center (such thick perinuclear actin bundles were observed in  $\sim 75\%$  of the videos analyzed). Fixation of the cells following

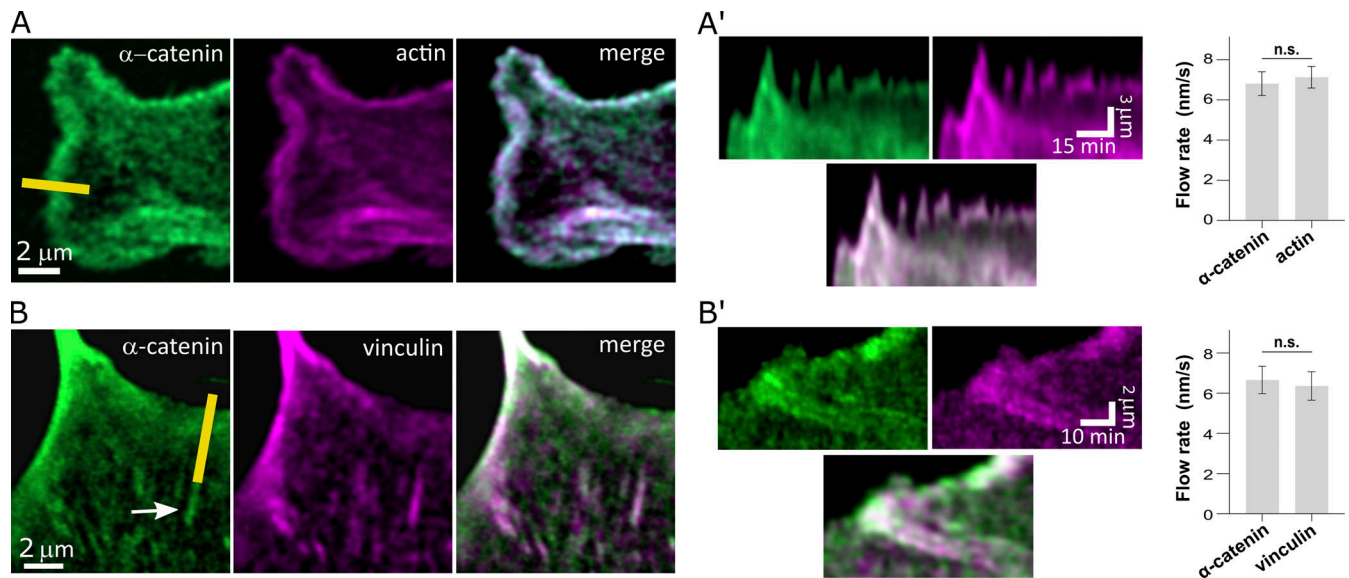


**Figure 2.  $\alpha$ -Catenin flows from the cell edge with actin and vinculin. (A and A')** Frame from a video of a cell expressing GFP- $\alpha$ -catenin and td-Tomato-Tractin showing colocalization of actin and  $\alpha$ -catenin at the edge; and kymographs taken from the yellow line (A'). The chart on the right shows quantifications of the flow rates of  $\alpha$ -catenin and actin in adhesions ( $n = 18$  adhesions in each case). **(B and B')** Average of six frames (equivalent to 2 min) from a video of a cell expressing GFP- $\alpha$ -catenin and mCherry-vinculin showing colocalization at the edge as well as in mature adhesions (arrow); and kymographs taken from the yellow line (B'). The chart on the right shows quantifications of the flow rates of  $\alpha$ -catenin and vinculin in adhesions ( $n = 24$  adhesions in each case). Statistical analysis for the flow rates was performed with two-tailed unpaired  $t$  test followed by Welch's correction.

overnight incubation and staining for F-actin revealed that over time, these bundles frequently collapsed, as evident by the appearance of dense wavy structures at the cell center (Fig. 3 E). This was in contrast to WT GFP- $\alpha$ -catenin, which rarely (<5%) formed perinuclear actin bundles and appeared primarily at the cell edges (in 85% of the cells,  $n = 20$  cells) and on stress fibers (although this was often obscured by cytoplasmic localization of the construct; ~60% of the cells; Fig. 3 E).

Notably, the enhanced localization of the L344P mutant in regions rich with actin stress fibers suggested that it could bind actin more efficiently compared with WT  $\alpha$ -catenin. To test this, we expressed a GFP-labeled fragment of  $\alpha$ -catenin corresponding to its ABD (amino acids 680–906; Nicholl et al., 2018) in the cells. Also, as proline is known to induce bending within  $\alpha$ -helices, we considered that the L344P mutation could potentially disrupt the structure of the second  $\alpha$ -helix present in the  $M_1$  domain of  $\alpha$ -catenin (Ishiyama et al., 2013), thereby giving rise to unknown structural changes in other areas of the protein. Hence, to verify that the observed effects of the L344P mutation were not due to  $\alpha$ -catenin misfolding, we added a mutant form of GFP- $\alpha$ -catenin in which the lysine at position 344 was replaced by alanine (GFP- $\alpha$ -catenin-L344A). Staining the cells for F-actin showed that in the majority of the transfected cells (>80%,  $n = 20$  cells in each case), the two mutated forms of  $\alpha$ -catenin displayed similar behavior to that of the L344P variant and were localized on stress fibers and in central regions of the cells, in the form of perinuclear actin bundles (Fig. 3 F). Taken together, the enhanced contrast between stress fiber and cytoplasmic localization of the three mutant forms, combined with the formation of irregular actin bundles in the presence of these mutants, suggest that “free”  $\alpha$ -catenin with an active ABD can

bind efficiently to stress fibers, potentially affecting their contractility. Interestingly, similar bundling was caused by the L344P and L344A mutants when expressed in vinculin<sup>-/-</sup> MEFs (Fig. S3 C), indicating that  $\alpha$ -catenin is primarily recruited to F-actin.

Collectively, these results demonstrate that the  $\alpha$ -catenin–vinculin interaction is necessary for normal cell spreading, regular protrusion/retraction cycles of the cell edge, sliding of integrin adhesions, and orderly formation of actin stress fibers. The mechanism by which the L344P mutant leads stress fibers to become highly contractile and aggregated at the cell center is not clear and should be addressed in future studies. One possibility is that the mere presence of  $\alpha$ -catenin enhances stress fiber contractility; hence, the sequestration of  $\alpha$ -catenin by vinculin in the adhesions could prevent excess  $\alpha$ -catenin translocation into the stress fibers, thereby attenuating excess contractility. Another possibility is that the poor connection between stress fibers and FAs in the presence of the L344P mutant inhibits the transmission of the contractile forces to the ECM, thereby leading to enhanced deformation of the stress fibers themselves, as predicted by our recent study (Feld et al., 2020).

### The $\alpha$ -catenin–vinculin interaction enhances force transmission to the matrix and FA maturation

The results described above indicate that vinculin may act as a clutch that engages with  $\alpha$ -catenin within integrin adhesions as the latter is bound to actin fibers. Indeed, introducing the L344P mutation in  $\alpha$ -catenin KD MEFs caused a noticeable disconnect between the respective flows of  $\alpha$ -catenin and vinculin (compare Figs. 2 B and 3 B). Quantification of the flow rates within adhesions showed that the  $\alpha$ -catenin–vinculin interaction attenuated the  $\alpha$ -catenin flow by approximately twofold ( $12.4 \pm 1.1$

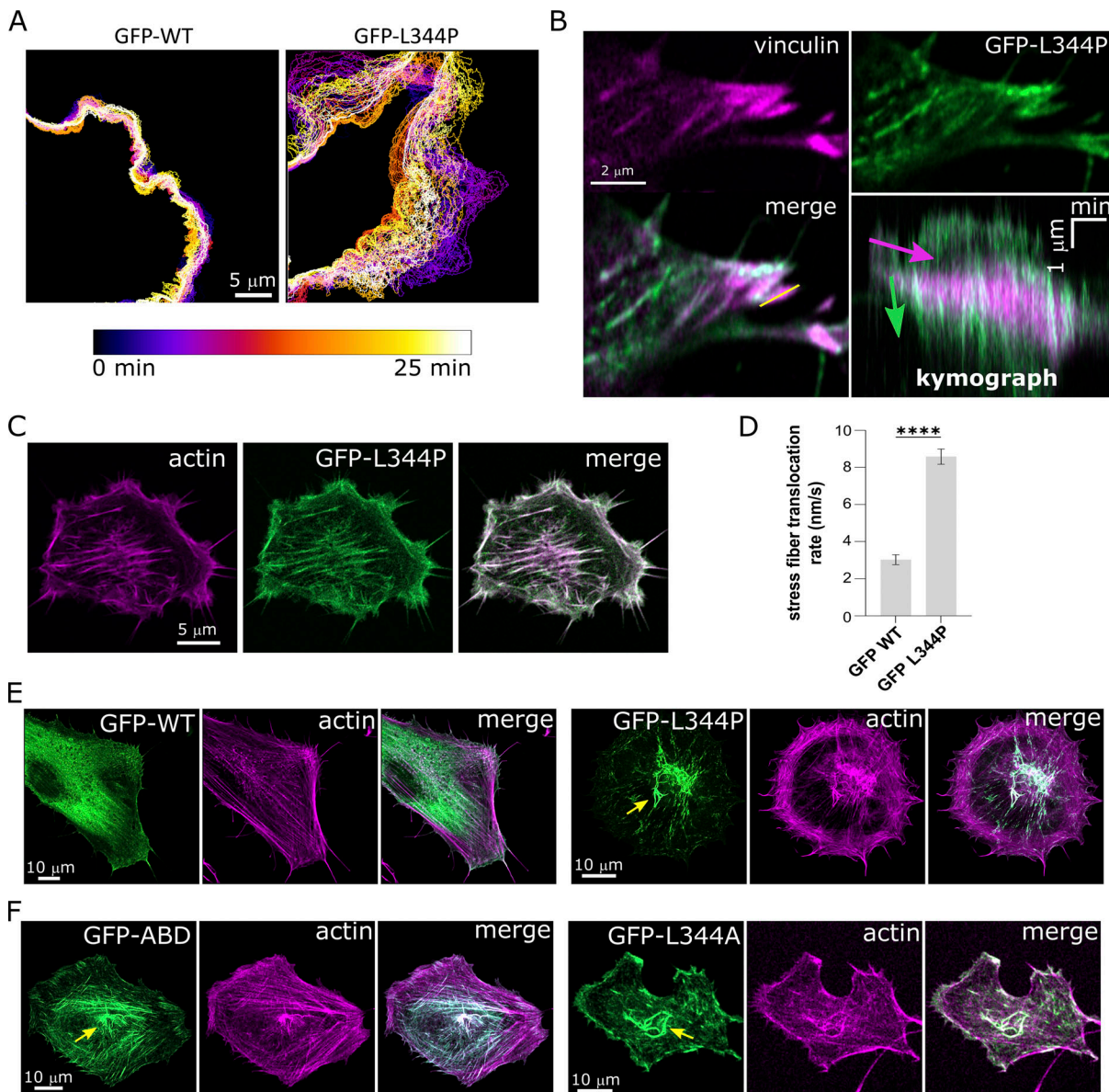


**Figure 3. The  $\alpha$ -catenin–vinculin interaction regulates cell edge activity and stress fiber formation.** (A) Color-coded time-series of the cell edge of  $\alpha$ -catenin KD cells expressing WT GFP- $\alpha$ -catenin (left) and GFP- $\alpha$ -catenin L344P (right), showing much higher cell edge activity in the latter. (B) Average of six frames (equivalent to 2 min) from a video zoomed-in on the edge of a cell expressing GFP- $\alpha$ -catenin L344P and mCherry-vinculin; the bottom right image is a kymograph taken from the yellow line shown in the bottom left image. Note the difference in speed (slope) between vinculin (purple arrow) and  $\alpha$ -catenin L344P (green arrow). (C) Frame from a video (Video 10) of an  $\alpha$ -catenin KD cell expressing GFP- $\alpha$ -catenin L344P and td-Tomato-Tractin, showing aggregation of both at the cell center. (D) Rate of translocation of stress fibers in cells expressing WT GFP- $\alpha$ -catenin and GFP- $\alpha$ -catenin L344P, as measured from kymographs specifically focused on transverse arc type of stress fibers.  $N > 25$  stress fiber retraction events from eight cells each. (E) Micrographs of  $\alpha$ -catenin KD cells expressing WT GFP- $\alpha$ -catenin and GFP- $\alpha$ -catenin L344P, stained for F-actin (phalloidin). The yellow arrows point to actin aggregates near the cell center. (F) Micrographs of  $\alpha$ -catenin KD cells expressing GFP-ABD and GFP- $\alpha$ -catenin L344A, stained for F-actin (phalloidin). The yellow arrows point to actin aggregates near the cell center. Statistical analysis for the stress fiber translocation rate was performed with two-tailed unpaired  $t$  test followed by Welch's correction (\*\*\*\*,  $P < 0.0001$ ).

and  $6.3 \pm 0.6$  nm/s for L344P and WT  $\alpha$ -catenin, respectively;  $n = 15$  each), thus reinforcing the idea that the  $\alpha$ -catenin–vinculin interaction acts as a clutch. Because stronger integrin–actin engagement leads to more efficient force transmission (Elosegui-Artola et al., 2016), we next set out to test the effect of the  $\alpha$ -catenin–vinculin interaction on force transmission to the matrix. To that end, we plated the cells on arrays of FN-coated pillars and measured the time-dependent deformation of the

pillars as a measure of force transmission (Feld et al., 2020). As shown in Fig. 4 A, WT MEFs gradually displaced the pillars over a period of  $\sim 10$  min, until they reached a plateau of  $\sim 120$  nm. In agreement with the adhesion maturation results, the  $\alpha$ -catenin KD cells displayed a significant decrease in matrix deformation (maximal displacement of  $\sim 40$  nm). Furthermore, WT GFP- $\alpha$ -catenin expression in  $\alpha$ -catenin KD cells restored pillar displacement almost completely (maximal displacement of

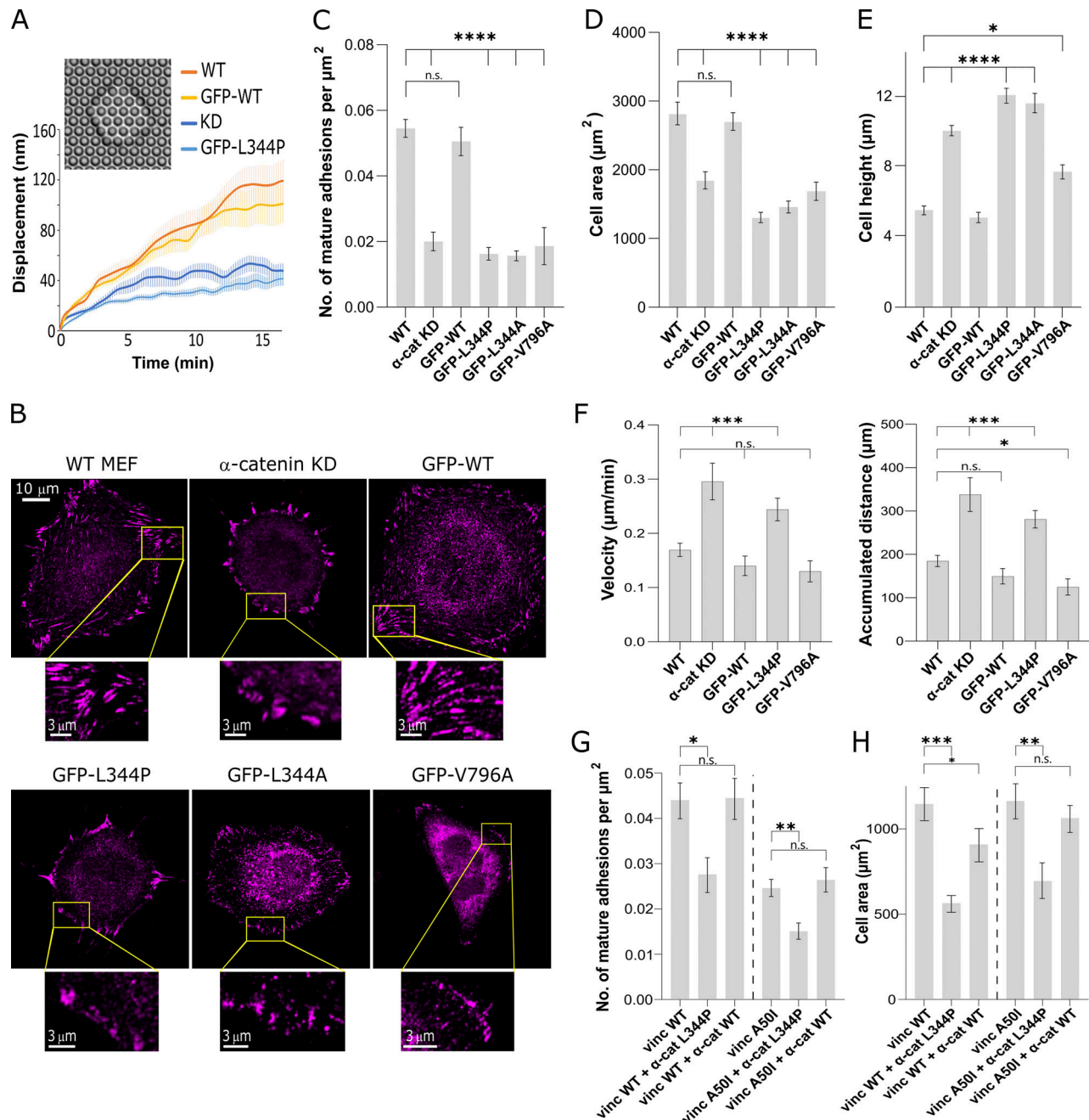


**Figure 4.  $\alpha$ -Catenin affects force transmission and adhesion maturation.** (A) Displacement as a function of time of 2- $\mu\text{m}$ -diameter FN-coated pillars by MEFs spreading on top of them (see example in inset image). The graphs shown are mean  $\pm$  SEM (in lighter hues).  $n > 30$  pillars in each case. (B) Micrographs of a WT MEFs,  $\alpha$ -catenin KD MEFs, and  $\alpha$ -catenin KD MEFs expressing WT GFP- $\alpha$ -catenin/GFP- $\alpha$ -catenin L344P/GFP- $\alpha$ -catenin L344A/GFP- $\alpha$ -catenin V796A, all immunostained for vinculin after 6 h of spreading on FN-coated coverslips (GFP channel not depicted). (C–E) Quantifications of the number of mature adhesions per square micrometer, cell areas, and cell heights of the six cell types 6 h after plating on FN-coated coverslips ( $n > 20$  cells in all cases). (F) Velocities and accumulated distances measured from MEF single-cell motility videos ( $n > 17$  cells in all cases). (G and H) Quantifications of the number of mature adhesions per square micrometer and areas of vinculin $^{-/-}$  MEFs expressing WT mCherry-vinculin or mCherry-vinculin A50I, alone or together with WT GFP- $\alpha$ -catenin or GFP- $\alpha$ -catenin L344P ( $n > 15$  cells in all cases). Statistical analysis of the adhesions, cell areas, cell heights, and cell motility (C–H) were tested by ANOVA followed by Tukey's post hoc test (\*,  $P < 0.05$ ; \*\*,  $P < 0.01$ ; \*\*\*,  $P < 0.001$ ; \*\*\*\*,  $P < 0.0001$ ).

~100 nm), whereas GFP- $\alpha$ -catenin-L344P expression did not (Fig. 4 A). These results strengthen the notion that  $\alpha$ -catenin-vinculin binding is a crucial clutch element within adhesions that is required for proper contractile activity and force transmission into the matrix.

As the growth of nascent adhesions into mature FAs is a force-dependent process (Galbraith et al., 2002; Riveline et al., 2001), we next sought to test the role of  $\alpha$ -catenin-vinculin interactions in FA maturation. To that end, we stained the cells for vinculin and F-actin after 6 h of spreading and found that

whereas WT MEFs formed mature vinculin-containing FAs,  $\alpha$ -catenin KD cells mostly did not display mature vinculin adhesions and had almost exclusively small adhesions (“focal complexes”) at the cell edge (Fig. 4, B and C). In line with the reduction in mature adhesions,  $\alpha$ -catenin KD cells failed to spread out and flatten, as evident by their reduced area (Fig. 4 D) and increased height (Fig. 4 E) compared with WT cells. Similarly, knocking down  $\alpha$ -catenin in NIH3T3 cells resulted in the formation of small adhesions and a decrease in cell spreading (Fig. S4, A–C). Expressing GFP- $\alpha$ -catenin in the  $\alpha$ -catenin KD MEFs restored the formation of mature FAs, while expressing GFP- $\alpha$ -catenin-L344P or L344A in the same cells did not (Fig. 4, B and C). Similar results were obtained when staining for zyxin (Fig. S4 D), a marker for mature FAs (Zaidel-Bar et al., 2003), confirming that the observed lack of mature vinculin-containing adhesions was not due to a lack of vinculin recruitment into mature adhesions, but rather due to the absence of such adhesions altogether. Furthermore,  $\alpha$ -catenin KD cells and cells expressing GFP- $\alpha$ -catenin-L344P or L344A were significantly smaller (Fig. 4 D) and less flat (Fig. 4 E) than WT cells or cells expressing WT GFP- $\alpha$ -catenin, which is consistent with their inability to form mature adhesions. To further test the relevance of the  $\alpha$ -catenin–vinculin interaction in the regulation of integrin adhesions, we used Matrigel (basement membrane-like) matrices, which were recently shown to induce the sliding of adhesions from the cell edge toward the center, resulting in highly elongated adhesions around the nucleus (Lu et al., 2020). We plated the cells on Matrigel-coated coverslips and stained them for vinculin after overnight incubation. This revealed that WT MEFs and WT GFP- $\alpha$ -catenin MEFs formed a significantly higher number of sliding adhesions than the  $\alpha$ -catenin KD cells and cells expressing GFP- $\alpha$ -catenin-L344P (Fig. S4 E).

Next, we expressed an  $\alpha$ -catenin variant in which valine 796—a key residue within the ABD—was replaced by alanine (V796A), as this mutant is known to reduce the binding of  $\alpha$ -catenin to actin (Ishiyama et al., 2018; see Fig. S4 F for verification of the expression levels of the mutant forms of  $\alpha$ -catenin). Cells expressing this mutant showed results (Fig. 4, B–E) similar to those of the  $\alpha$ -catenin KD cells and the other mutants, confirming that the actin-binding ability of  $\alpha$ -catenin is important for adhesion maturation. Interestingly, single-cell motility assays showed that  $\alpha$ -catenin KD cells and cells expressing the L344P mutant were more motile than the WT controls, as evident by their increased distances and velocities (Fig. 4 F). In contrast, V796A mutant cells displayed a motility phenotype similar to that of WT controls (Fig. 4 F), despite displaying adhesion and cell size phenotypes comparable to the KD and L344P cells (Fig. 4, C–E). This disengagement of phenotypes points to a complex relationship between the strength of  $\alpha$ -catenin–F-actin binding, adhesion reinforcement, and cell migration, which should be investigated in more depth in future studies.

As a major axis of vinculin recruitment to FAs is through its binding to talin, we set out to test the effects of this interaction on adhesion growth in the context of the  $\alpha$ -catenin–vinculin interaction. To that end, we transfected vinculin<sup>-/-</sup> MEFs with WT mCherry–vinculin or mCherry–vinculin-A50I, a mutant form of vinculin that has reduced binding to talin compared

with WT vinculin, but is still recruited to adhesions (Cohen et al., 2006). We coexpressed WT GFP- $\alpha$ -catenin or GFP- $\alpha$ -catenin-L344P constructs in these cells. As expected, the A50I mutation led to the formation of less mature adhesions compared with WT vinculin (Fig. 4 G). Moreover, coexpression with the L344P mutant led to a further decrease in adhesion sizes, which was accompanied by a reduction in cell area (Fig. 4 H). These results indicate that once vinculin is recruited to adhesions (through talin or other adhesion proteins), its interaction with  $\alpha$ -catenin is essential for the regulation of adhesion maturation and cell spreading.

Taken together, these results show that the  $\alpha$ -catenin–vinculin interaction plays a critical role in integrin adhesion regulation, constituting an important addition to the classic adhesion maturation model through the talin–vinculin module. In this process, forces that are transmitted through the adhesions lead to stretching of the talin molecules, thereby exposing hidden vinculin binding sites (del Rio et al., 2009). When vinculin is recruited to those sites, it reinforces the link between the cytoplasmic tails of the integrins and F-actin, thereby stabilizing the adhesions (Elosegui-Artola et al., 2016). Although the relevance of this model to the behavior of cells on soft and stiff matrices is still being debated (Driscoll et al., 2020), the talin–vinculin module is clearly important for adhesion regulation and mechanosensing of the ECM. Importantly, our results show that although vinculin has an ABD, its ability to bind to  $\alpha$ -catenin is equally vital for proper interaction with F-actin, and consequently for proper force transmission and adhesion maturation.

### $\alpha$ -Catenin regulates rigidity-dependent cell growth following EMT

The results presented until now raised the question of whether the role played by  $\alpha$ -catenin in regulation of integrin adhesions could be affected by the presence of cadherin-based cell–cell adhesions in the cells. To address this, we studied MEFs that were in contact with one another (mesenchymal cell–cell) as well as with the matrix. We observed the presence of  $\alpha$ -catenin,  $\beta$ -catenin, and N-cadherin in the mesenchymal cell–cell contacts and found that  $\beta$ -catenin (but not N-cadherin) was also present at the lamellipodia along with  $\alpha$ -catenin (Fig. S5 A). Still, in such cells, mature vinculin-containing FAs formed in lamellipodial regions containing  $\alpha$ -catenin (Fig. S5 A), suggesting that  $\alpha$ -catenin can affect both cell–cell and cell–matrix adhesion regulatory processes within the same cell. The extent of this effect might depend on the cell type. For instance, in epithelial layers, where cells are linked through AJs, recruitment of  $\alpha$ -catenin to integrin adhesions might be prevented, thereby inhibiting the formation of mature FAs. In support of this, we found a gradual increase in the cell edge localization of  $\alpha$ -catenin when we used TGF $\beta$  to induce the EMT of the epithelial Madin–Darby canine kidney (MDCK) cell line (Fig. 5 A).

To further address this, we set out to test whether  $\alpha$ -catenin was involved in the induction of EMT, particularly in the context of matrix rigidity, which was shown to be a positive regulator of the process (Wei et al., 2015). To that end, we used WT MDCK cells as well as an MDCK variant in which  $\alpha$ -catenin expression

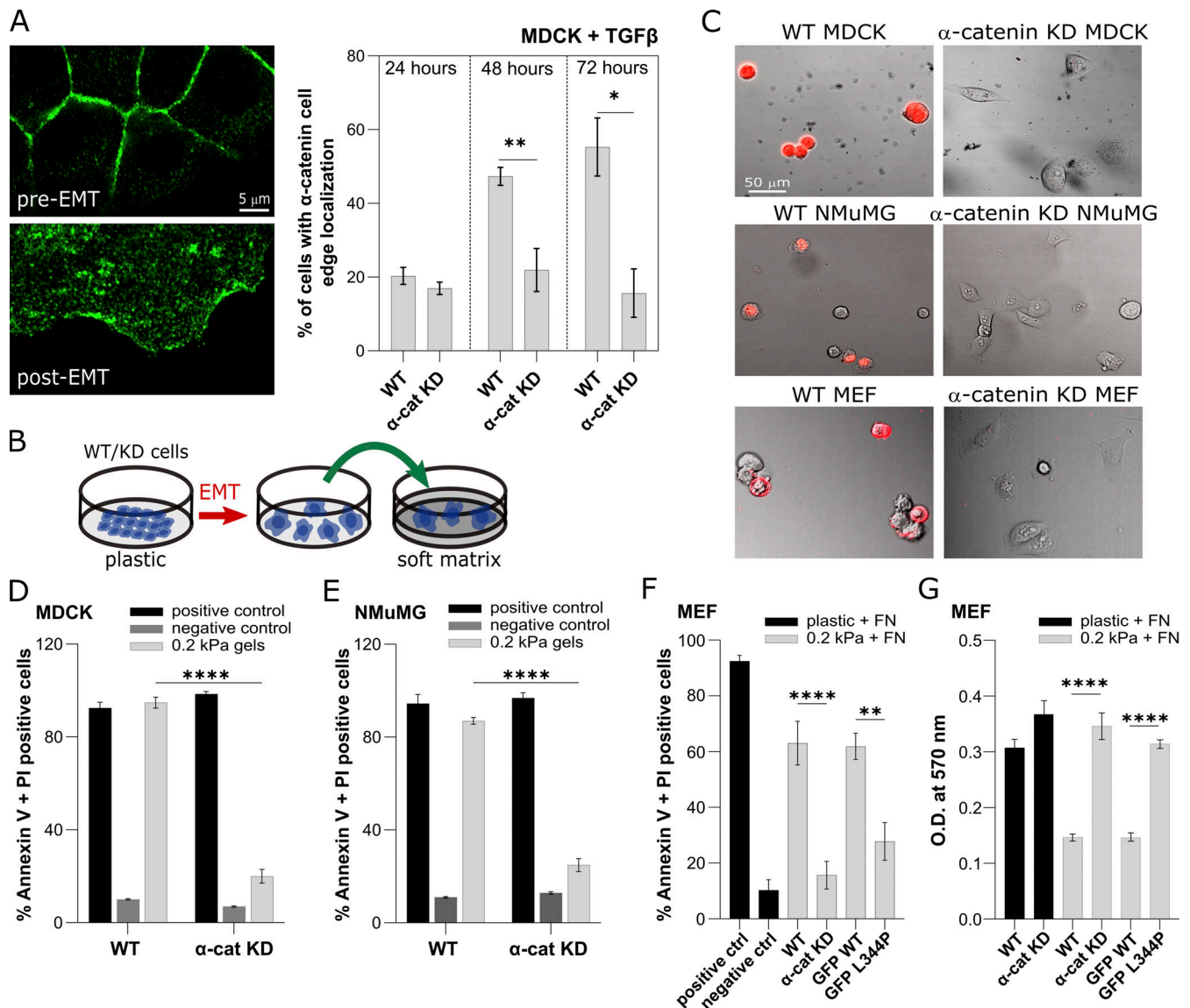


**Figure 5. Lack of  $\alpha$ -catenin–vinculin interaction endows cells with rigidity-independence.** (A) Left:  $\alpha$ -Catenin staining in WT MDCK cells before and after EMT. Right: Quantification of the percentage of cells with  $\alpha$ -catenin cell edge localization 24, 48, and 72 h after the addition of TGF- $\beta$ . (B) Schematic of the experiment designed to test  $\alpha$ -catenin’s role in rigidity dependence after EMT in MDCK and NMuMG cells. (C) Representative images of MDCK, NMuMG (after EMT), and MEF cells stained with Annexin-FITC on 0.2-kPa gels coated with FN, 6 h after plating (PI staining not depicted). (D) Quantification of the percentage of Annexin V- and PI-positive WT and  $\alpha$ -catenin KD MDCK cells on 0.2-kPa gels coated with FN. (E) Quantification of the percentage of Annexin V- and PI-positive WT and  $\alpha$ -catenin KD NMuMG cells on 0.2-kPa gels coated with FN. (F) Quantification of the percentage of Annexin V- and PI-positive WT MEFs,  $\alpha$ -catenin KD MEFs, and  $\alpha$ -catenin KD MEFs expressing WT GFP- $\alpha$ -catenin or GFP- $\alpha$ -catenin L344P, plated for 24 h on 0.2-kPa FN-coated matrices. (G) MTT measurement of WT MEFs,  $\alpha$ -catenin KD MEFs, and  $\alpha$ -catenin KD MEFs expressing WT GFP- $\alpha$ -catenin or GFP- $\alpha$ -catenin L344P, plated for 24 h on 0.2-kPa FN-coated matrices. In the Annexin/PI graphs, positive and negative controls, the cells were heated at 65°C for 15 min for the former and left untreated for the latter and plated on FN-coated plastic ibidi wells. For the MTT assay, the positive growth control refers to WT and  $\alpha$ -catenin KD MEF cells plated on a FN-coated 96-well plate (plastic). Statistical analysis of the  $\alpha$ -catenin cell-edge localization (A) was tested by nested ANOVA followed by Tukey’s post hoc test, and percentage of apoptotic cells and MTT assay (D–G) were tested by ANOVA followed by Tukey’s post hoc test (\*,  $P < 0.05$ ; \*\*,  $P < 0.01$ ; \*\*\*\*,  $P < 0.0001$ ).

was stably knocked down (Benjamin et al., 2010; Fig. S5 B). First, to test the effect of  $\alpha$ -catenin KD, we grew the cells for 48 h on FN-coated glass coverslips and quantified the expression of E-cadherin, vimentin, and  $\alpha$ -smooth muscle actin ( $\alpha$ -SMA). WT MDCKs displayed a strong epithelial phenotype with tight E-cadherin connections between the cells and very low vimentin levels (Fig. S5 C).  $\alpha$ -Catenin KD MDCK cells were less tightly packed compared with the WT cells and displayed E-cadherin

adhesions, accompanied with a slight increase in vimentin and  $\alpha$ -SMA intensity (Fig. S5, C and D). These results indicated that the loss of  $\alpha$ -catenin was not sufficient for the cells to undergo complete EMT (which was observed only upon treatment with TGF $\beta$ ; Fig. S5 D). We next tested if the absence of  $\alpha$ -catenin could affect EMT occurrence as a function of matrix rigidity. To that end, we plated both cell lines on soft (0.2 kPa) and stiff (25 kPa) FN-coated substrates for 3 h, before adding TGF $\beta$  to the plates.

After a 72-h incubation, WT cells on the soft matrix remained epithelial (Fig. S5 E), whereas on the stiff matrix, the cells formed colonies that were less tightly packed, with cells that were detached from the colonies at the periphery (Fig. S5 E, yellow arrows), indicative of partial EMT. Interestingly, on soft matrices the KD cells also displayed a partial EMT phenotype, while on stiff matrices they underwent complete EMT, as evident by the complete loss of cell-cell contacts and spindle-like morphologies characteristic of mesenchymal cells (Fig. S5 E). Thus, although the baseline phenotypes of WT and  $\alpha$ -catenin KD MDCK cells on soft matrices differed in the presence of TGF $\beta$  (fully epithelial and partial EMT, respectively), stiff matrices shifted both cell types toward the mesenchymal state (partial EMT and complete EMT, respectively). Still, the transition to partial EMT on soft surfaces was enabled only when  $\alpha$ -catenin was absent from the cells (Fig. S5 E), suggesting an important role for  $\alpha$ -catenin in sensing soft matrices.

To test the role of  $\alpha$ -catenin in mechanosensing also at the mesenchymal state, we focused on the induction of apoptosis in response to soft matrices, which normally occurs when cells fail to properly attach and spread (Zhang et al., 2011). To that end, we induced EMT of WT and  $\alpha$ -catenin KD MDCK cells in plastic dishes and then transferred them onto soft (0.2-kPa) FN-coated substrates (Fig. 5 B). Remarkably, Annexin V and PI staining showed that only ~20% of  $\alpha$ -catenin KD MDCK cells activated apoptosis 6 h after plating, compared with ~95% of WT MDCK cells (Fig. 5, C and D). We observed similar results with normal murine mammary gland (NMuMG) cells, another epithelial cell line, after knocking down the expression of  $\alpha$ -catenin (Fig. 5, C and E; and Fig. S5 B). Furthermore,  $\alpha$ -catenin KD and the L344P mutation in the MEFs both led to apoptosis inhibition on 0.2-kPa FN-coated surfaces, compared with WT controls (Fig. 5, C and F). Importantly, using the MTT assay we verified that while WT MEFs and MEFs expressing WT GFP- $\alpha$ -catenin failed to proliferate on the 0.2-kPa surfaces,  $\alpha$ -catenin KD and L344P mutant cells were able to proliferate on such matrices (Figs. 5 G and S5 F).

Notably, the observed avoidance of apoptosis and ability to grow on soft matrices by  $\alpha$ -catenin KD and L344P mutant cells was accompanied by enhanced cell spreading (Figs. 5 C and S5 F), which was in contrast to the behavior of the same cells on stiff surfaces (Fig. 4, B and D). We propose that this discrepancy could be explained by the low rate of nascent adhesion turnover on soft matrices compared with stiff ones (Changede et al., 2015). On stiff matrices, the impaired connection between integrins and F-actin in absence of  $\alpha$ -catenin or the presence of the L344P mutant leads to slower force loading, which prevents the mechanosensitive adhesion proteins (e.g., talin) from experiencing high enough forces, thus precluding rapid adhesion reinforcement through recruitment of additional proteins (vinculin) into the adhesions. Hence, the adhesions disassemble before recruitment occurs, and on average the cells are left with small, immature adhesions, and they spread poorly. In contrast, the slow disassembly rate of nascent adhesions on soft surfaces provides sufficient time for the adhesions to grow without disassembling despite the slow force loading in  $\alpha$ -catenin KD or L344P mutant cells. Therefore, we propose that adhesion growth

does not depend solely on the contractile activity that is transmitted through the adhesions to the ECM per se, but rather depends on the balance between cellular force loading and the external rigidity. This can affect downstream cellular decisions, whereby large adhesions support cell survival and proliferation, as in the case of WT cells on stiff matrices or  $\alpha$ -catenin KD/L344P-expressing cells on soft matrices (Fig. 5 G; see also Amer et al. [2021]). Notably, this might be important also for understanding the involvement of  $\alpha$ -catenin in cancer, which is classically associated with its role in the maintenance of AJs (Bajpai et al., 2009) and/or its involvement in cytoplasmic sequestration of pro-proliferative transcriptional regulators (Piao et al., 2014; Silvis et al., 2011). Our findings add an additional layer to this picture, as they indicate that  $\alpha$ -catenin regulates integrin adhesions and mechanosensing, which are directly linked to anchorage independence (Wolfenson et al., 2016; Meacci et al., 2016; Yang et al., 2019), a hallmark of cancer cells (Guadamillas et al., 2011).

## Materials and methods

### Cell culture, reagents, and transfections

WT MEFs (referred to in other publications as RPTP $\alpha^{+/+}$  cells) were isolated from embryonic day 13 (E13)–E15 WT embryos and underwent spontaneous immortalization (Su et al., 1999). NIH3T3 (#CRL-1658; ATCC), WT MDCK (#CCL-34; ATCC), and MDCK  $\alpha$ -catenin KD (generated from the WT MDCK by shRNA [Benjamin et al., 2010]) were received from MBI Singapore cell collection. Vinculin $^{-/-}$  MEFs were obtained from Benny Geiger's lab (Weizmann Institute of Science), originally generated from vinculin $^{-/-}$  mice provided by E.D. Adamson (Burnham Institute, La Jolla, CA; Xu et al., 1998). NMuMG cells (#CRL1636; ATCC) were received from Yaron Antebi's lab (Weizmann Institute of Science). All cells were cultured at 37°C in a 5% CO<sub>2</sub> incubator in DMEM supplemented with 10% FBS and 100 IU/ml penicillin-streptomycin (all reagents were from Biological Industries). Recombinant TGF $\beta$  (10 ng/ml) was purchased from Peprotech (#100-21). For EMT experiments, the cells were treated with TGF $\beta$  for 48–72 h. Transfections were carried out 1 d before measurements using the NEPA21 Electroporator (Nepa Gene) according to the manufacturer's instructions, with ~10<sup>6</sup> cells per reaction and 10  $\mu$ g DNA.

### Plasmids and shRNA oligonucleotides

The plasmids for GFP/mCherry-tagged  $\alpha$ -catenin (Seddiki et al., 2018),  $\alpha$ -actinin (Hirata et al., 2014), and vinculin (#55160; Addgene), as well as the tdTomato-Tractin plasmid (Belin et al., 2014), were obtained from MBI Singapore. The L344P, L344A, and V796A mutations were inserted into the GFP- $\alpha$ -catenin plasmid using the Q5 Site-Directed Mutagenesis Kit (New England Biolabs).

Lentiviral KD of  $\alpha$ -catenin was performed using the SHCLNG-NM\_009818 MISSION shRNA plasmid (Merck) targeting the sequence 5'-CCGGCCAGGAGTTTACACAGAGAACTCGAGTTCTCTGTGTAACCTCTGGCTTTTGG-3'; control cells were generated using the SHC202—MISSION TRC2 pLKO.5-puro Non-Mammalian shRNA Control Plasmid (Merck). After

infection, cells were grown in 1 and 4  $\mu\text{g}/\text{ml}$  puromycin for MDCK and MEF, and KD was tested using Western blotting (WB) and immunofluorescence measurements.

### Pillars, soft gel fabrication, and cell spreading

Molds for pillar fabrication were generated by high-resolution photolithography, using a  $5\times$  reduction autostepper (GCA Autostep 200 DSW i-line, Integrated Solutions) to pattern the photoresist. A  $\text{C}_4\text{F}_8/\text{SF}_4$ -based deep reactive ion etch was performed on the wafers to etch holes to the desired depth. After stripping the photoresist, the silicon masters were cleaned and then silanized with (tridecafluoro-1,1,2,2-tetrahydrooctyl)-1-trichlorosilane (#T2492; United Chemical Technologies) overnight under vacuum (Ghassemi et al., 2012). Pillars were fabricated by pouring polydimethylsiloxane (PDMS; Sylgard 184, Dow Corning; mixing ratio 10:1) into the molds. The molds were then placed, face down, onto glass-bottom 35-mm dishes (#0 coverslip; Cellvis) which were incubated at  $65^\circ\text{C}$  for 12 h to cure the PDMS. The molds were immersed in ethanol to prevent pillar collapse and pried off the dish. The ethanol was replaced with PBS by serial dilutions. Human plasma full-length FN (#FC010-10MG; Merck) was added to the dish at a final concentration of  $10\ \mu\text{g}/\mu\text{l}$  for 1-h incubation at  $37^\circ\text{C}$ . Next, residual FN was washed away by replacing the solution with HBSS (#03-025-1B; Biological Industries) supplemented with 20 mM HEPES (#02-018-1A; Biological Industries), pH 7.2, or PBS.

All pillars had a diameter of  $2\ \mu\text{m}$  and a height of  $13.2\ \mu\text{m}$ . These pillars were used to measure the long-term time-dependent forces that are generated after initial formation and reinforcement of the adhesions (Wolfenson et al., 2016; Ghassemi et al., 2012). The center-to-center spacing between pillars was  $4\ \mu\text{m}$ . Pillar bending stiffness,  $k_{\text{ECM}}$ , was calculated by Euler-Bernoulli beam theory:

$$k_{\text{ECM}} = \frac{3\pi ED^4}{64 L^3},$$

where  $D$  and  $L$  are the diameter and length of the pillar, respectively, and  $E$  is the Young's modulus of the material (2 MPa for the PDMS used here). The 0.2- and 25-kPa substrates were fabricated by using Sylgard 52-276 at ratios of 2:1 and 1:2.7, respectively, according to the measurements performed previously (Ou et al., 2016).

### Pillar displacement measurements

1 d before the pillar experiments, cells were sparsely plated to minimize cell-cell interactions before replating. The next day, cells were trypsinized, centrifuged with growth medium, re-suspended, and preincubated in HBSS/HEPES at  $37^\circ\text{C}$  for 30 min before the experiment. Cells were then spread on the FN-coated pillars. In all cases, we made sure that the cells were isolated when plated on the substrates.

Time-lapse imaging of cells spreading on the pillars was performed using an inverted microscope (Leica DMIRE2) at  $37^\circ\text{C}$  using a  $63\times$  1.4-NA oil-immersion objective. Bright-field images were recorded every 10 s with a Retiga EXi Fast 1394 charge-coupled device camera (QImaging). The microscope and camera were controlled by Micromanager software (Edelstein et al.,

2010). For each cell, a video of 1–3 h was recorded. To minimize photo damage to the cells, a 600-nm longpass filter was inserted into the illumination path.

Tracking of pillar movements over time was performed with ImageJ (National Institutes of Health) using the Nanotracking plugin, as described previously (Wolfenson et al., 2016). In short, the cross-correlation between the pillar image in every frame of the video and an image of the same pillar from the first frame of the video was calculated, and the relative  $x$  and  $y$  position of the pillar in every frame of the video was obtained. To consider only movements of pillars from their zero position, we analyzed only pillars that at the start of the video were not in contact with the cell and that were reached by the cell edge during the video. Drift correction was performed using data from pillars far from any cell in each video. For each pillar, the displacement curve was generated by Matlab (vR2017a; MathWorks).

### Immunoblotting and immunoprecipitation

For immunoblots, ice-cold PBS was used to wash the cells. The cells were lysed using radioimmunoprecipitation assay buffer (Tris-HCl 10 mM, 1% SDS, 10 mg/ml deoxycholate, 150 mM NaCl, 1% NP-40, and protease inhibitors cocktail [Roche]). The total protein samples were separated using 12% SDS-PAGE and transferred onto nitrocellulose membranes (Bio-Rad). The membranes were blocked using 5% milk and incubated with primary antibodies overnight at  $4^\circ\text{C}$  for mouse anti- $\alpha$ -catenin (1:1,000, sc-9988; Santa Cruz) and mouse anti-GAPDH (1:10,000, #ab8245; Abcam) as a loading control. Next, the membranes were exposed to peroxidase-conjugated goat anti-mouse IgG (1:10,000, #AB\_2338504; Jackson ImmunoResearch) for 1 h at room temperature. The EZ-ECL Enhanced Chemiluminescence Detection Kit (#1705061; Bio-Rad Laboratories) was used to visualize and analyze the protein bands.

For immunoprecipitation, the cell lysates were incubated with  $3\ \mu\text{g}$  of anti-vinculin (#700062; Thermo Fisher Scientific) and  $3\ \mu\text{g}$  of anti- $\alpha$ -catenin (sc-9988; Santa Cruz) in immunoprecipitation buffer (20 mM Tris-HCl, pH 7, 0.3 M NaCl, 2 mM EDTA, and 1% NP-40) containing 0.2 mM 4-(2-aminoethyl) benzenesulfonyl fluoride hydrochloride (#101500; Calbiochem) overnight at  $4^\circ\text{C}$  and then rotated with Pierce Protein G Magnetic Beads (#88848; Thermo Fisher Scientific) for 1 h at  $4^\circ\text{C}$ . Protein complexes were washed three times in PBS and subsequently extracted with  $1\times$  SDS loading buffer for 3 min at  $95^\circ\text{C}$ . SDS-PAGE, WB, and enhanced chemiluminescence analyses were performed as discussed above.

### Immunofluorescence microscopy

For immunofluorescence microscopy, cells were plated on FN-coated coverslips or Matrigel-coated Ibidi 8-well chamber slides and fixed with 4% PFA (#47608; Sigma-Aldrich) supplemented with 0.2% Triton X-100 (#T8787; Sigma-Aldrich) in PBS. Blocking was performed using 3% BSA (#A4503; Sigma-Aldrich) and 0.2% Triton X-100 in PBS for 1 h at RT. Immunolabeling was performed with primary antibodies against mouse anti- $\alpha$ -catenin (1:300, sc-9988; Santa Cruz), rabbit anti-vinculin (1:500, #700062; Thermo Fisher Scientific), rat anti-E-cadherin (1:300, #U3254; Merck), rabbit anti- $\alpha$ -actinin (1:500, #ab108198;

Abcam), rabbit anti-zyxin (1:100, received from Benny Geiger's lab, generated in-house [Chorev et al., 2014]), chicken anti-vimentin (1:500, #ab24525; Abcam), rabbit anti-N-cadherin (1:200, #ab18203; Abcam), rabbit anti- $\beta$ -catenin (1:200, #C2206; Sigma-Aldrich) and rabbit anti- $\alpha$ -SMA (1:200, #A2547; Cell Marque) overnight at 4°C. The cells were washed three times with PBS followed by the addition of goat anti-rat Alexa Fluor 405-conjugated secondary antibody (1:500, #ab175661; Abcam), donkey anti-rabbit Alexa Fluor 488-conjugated secondary antibody (1:500, #ab150061; Abcam), goat anti-rat IgG Alexa Fluor 488-conjugated secondary antibody (1:500, #A-11006; Thermo Fisher Scientific), goat anti-mouse Alexa Fluor 555-conjugated secondary antibody (1:500, #ab150118; Abcam), goat anti-chicken Alexa Fluor 555-conjugated secondary antibody (1:500, #ab150170; Abcam), donkey anti-rabbit Alexa Fluor 647-conjugated secondary antibody (1:500, #ab150067; Abcam), goat anti-mouse Alexa Fluor 647-conjugated secondary antibody (1:500, #ab150119; Abcam), phalloidin Alexa Fluor 488 (1:500, #A12379; Thermo Fisher Scientific), phalloidin Alexa Fluor 555 (1:500, #A34055; Thermo Fisher Scientific), phalloidin Alexa Fluor 647 (1:500, #A22287; Thermo Fisher Scientific), and phalloidin-iFluor 594 Reagent (1:1,000, #ab176757; Abcam) for 1 h at RT in the dark. After washing the secondary antibodies three times with PBS, ProLong Gold Antifade reagent was added to mount the coverslips. Images were then taken at RT with a Zeiss LSM800 confocal microscope using a 20 $\times$  0.9-NA air objective (Fig. 5 C) and 63 $\times$  1.4-NA oil objective controlled by Zen imaging software (Zeiss).

### Image analyses and quantifications

Analyses of the cell area and number of mature and sliding adhesions were performed using a home-built Fiji macro (National Institutes of Health). The confocal images were subjected to an intensity threshold to select the cell area using the phalloidin channel, and the “analyze particles” tool was used to measure the area of the cell. To account for mature adhesions, a cell mask was generated that measured the cell area from a distance of 2  $\mu$ m from the cell edge on all sides. The number of adhesions in the cell center was calculated using the “analyze particle” tool after thresholding the vinculin channel.

### EMT experiments

The MDCK WT, MDCK  $\alpha$ -catenin KD, NMuMG WT, and  $\alpha$ -catenin KD were sparsely plated on FN-coated 0.2- and 25-kPa gels. 3 h after plating, EGF (50 ng/ml) or TGF $\beta$  (10 ng/ml) was added to the medium and left for 48–72 h before fixation and staining. In another set of experiments, the cells were made to undergo EMT on plastic and then plated on the FN-coated 0.2-kPa PDMS gels.

### Cell viability assays

The cell viability of the MEFs was assessed using the MTT assay (#M5655; Merck).  $1 \times 10^4$  cells were seeded on FN-coated plastic and 0.2-kPa gels in 96-well plates and incubated in DMEM. After 24 h, the MTT reagent was added to the cells at a final concentration of 0.5 mg/ml and incubated at 37°C for 3 h. The DMEM was removed, and 10% SDS in 0.1 M HCl was added to dissolve

the crystals. The amount of MTT formazan product was measured at 570 nm using a microplate reader.

### Apoptosis assays

The apoptosis assay was performed using the Annexin V-FITC Apoptosis Staining/Detection Kit (#14085; Abcam).  $1 \times 10^4$  cells were seeded on FN-coated plastic and 0.2 kPa gels on Ibidi 8-well chamber slides. For the positive and negative controls, the cells were heated at 65°C for 15 min (positive) and left untreated (negative) and plated on FN-coated plastic Ibidi wells. 6 h after plating, 10  $\mu$ l of FITC-Annexin V and 10  $\mu$ l of propidium iodide (PI) were added to the cells for 15 min and incubated in the dark. The staining of the apoptotic cells (Annexin V + PI positive) were assessed using Zeiss LSM800 confocal microscope with a 20 $\times$  0.9-NA air objective.

### Single-cell motility assay

The cells were incubated with 400 nM of SiR-DNA (#SC007; Spirochrome) in full DMEM, overnight at 37°C in a 5% CO<sub>2</sub> incubator. The cells were then trypsinized, centrifuged, and resuspended in colorless DMEM.  $1 \times 10^4$  cells were plated in each well of a FN-coated glass-bottom 24-well plates (#P24-0-N; Cellvis) and incubated at 37°C for 1 h. The cells were then imaged at 10 $\times$  magnification every 15 min at 37°C and 5% CO<sub>2</sub> using an ImageXpress micro system (Molecular Devices). Quantifications were performed using the Manual Tracking plugin in Fiji and the Chemotaxis and Migration Tool (Ibidi, downloaded from: <https://ibidi.com/chemotaxis-analysis/171-chemotaxis-and-migration-tool.html>).

### RNA extraction and quantitative real-time PCR (qRT-PCR)

RNA was extracted from cultured cells using PureLink RNA Mini Kit (12183018A; Invitrogen), and reverse transcription was performed with qScript cDNA Synthesis Kit (95047-100; Quanta Biosciences). In qRT-PCR experiments, 10 ng cDNA was used, and PCR products were detected using Fast SYBR Green Master Mix (4385614; Applied Biosystems). Expression results were normalized to *Gapdh* and to the indicated control groups (relative quantification =  $2^{-\Delta\Delta Ct}$ ; Ct, threshold count). The primers used are listed in Table 1.

### Live-cell imaging

Transfected  $\alpha$ -catenin KD cells were trypsinized, centrifuged with growth medium (DMEM), resuspended, and preincubated in HBSS/Hepes at 37°C for 5 min. These cells were then plated on FN-coated coverslips held in a ChamSlide CMS coverslip holder, and live-cell images were taken with a Zeiss LSM800 confocal microscope using a 63 $\times$  1.4-NA objective at intervals of 20 s.

### Statistical analysis

All experiments were repeated at least twice on separate days using duplicates and triplicates on each day. The statistical analysis was carried out with the help of GraphPad Prism (v9.0.0). All quantifications represent the mean  $\pm$  SEM. Two-tailed unpaired *t* test with Welch's correction was used for group comparisons whereas multiple group comparisons were performed by ANOVA followed by Tukey's post hoc test, as

Table 1. List of primers

Primer	Forward	Reverse
<b>Murine</b>		
<i>Ctnna1</i>	5'-TCTCTACTGCCACCAGCTCAAC-3'	3'-AAGCCATCCCCTGTGACTTCT-5'
<i>Ctnna2</i>	5'-ACCCATGACATTACAGCGAG-3'	3'-CACGTGTGCAGGAGGAATCT-5'
<i>Hprt</i>	5'-GTTGGGCTTACCTCACTGCT-3'	3'-TAATCACGACGCTGGGACTG-5'
<i>Gapdh</i>	5'-GGGTCCCAGCTTAGGTTTCATC-3'	3'-TACGGCCAAATCCGTTTACA-5'
<b>Canine</b>		
<i>CTNNA1</i>	5'-AAGCTGGATGCTGAGGTGTC-3'	3'-TCGGACGTGTTCTTGAGTGG-5'
<i>CTNNA2</i>	5'-AAACTCCCACCGACCCATAG-3'	3'-TGGTGTGACAAGGGTCGTC-5'
<i>HPRT1</i>	5'-CGCTGAGGATTTGGAAAAAGTG-3'	3'-TTGAGCACACAGGGGCTAC-5'
<i>GAPDH</i>	5'-GTAGTGAAGCAGGCATCGGA-3'	3'-GTCGAAGGTGGAAGAGTGGG-5'

indicated in the figure legends. Differences were considered to be statistically significant from a P value <0.05.

### Online supplemental material

**Fig. S1** shows that the dominant  $\alpha$ -catenin isoform that is expressed in the MEFs is  $\alpha$ E-catenin, and that  $\alpha$ -catenin is recruited to the cell edge in the absence of vinculin or  $\alpha$ -actinin. It also shows the enrichment of  $\alpha$ -catenin in regions containing actin stress fibers. **Fig. S2** shows the lack of colocalization of  $\alpha$ -actinin and  $\alpha$ -catenin. **Fig. S3** shows the co-IP of  $\alpha$ -catenin and vinculin, the ruffling of the cell edge in the absence of  $\alpha$ -catenin-vinculin interaction, and the bundling of  $\alpha$ -catenin in the center of vinculin<sup>-/-</sup> MEFs. **Fig. S4** shows that knocking down  $\alpha$ -catenin in NIH3T3 cells results in formation of small adhesions and a decrease in cell spreading, and that the lack of  $\alpha$ -catenin-vinculin interaction prevents formation of mature zyxin-containing FAs on FN-coated coverslips or formation of sliding adhesions when MEFs are plated on Matrigel. It also shows confirmation of the expression of the  $\alpha$ -catenin mutants on the background of  $\alpha$ -catenin KD. **Fig. S5** shows the presence of  $\alpha$ -catenin along with  $\beta$ -catenin at the cell edge, and that FAs form in lamellipodial regions containing  $\alpha$ -catenin in cells that also contain cell-cell junctions. It also shows the effects of  $\alpha$ -catenin KD on the EMT state of MDCK cells and the difference in spreading on soft gels in the presence of WT  $\alpha$ -catenin and  $\alpha$ -catenin-L344P. **Video 1** is a time-lapse confocal fluorescence video showing the spreading of an  $\alpha$ -catenin KD MEF expressing tdTomato-Tractin and WT GFP- $\alpha$ -catenin. **Video 2** is a time-lapse confocal fluorescence video showing the spreading of an  $\alpha$ -catenin KD MEF expressing mCherry- $\alpha$ -actinin and WT GFP- $\alpha$ -catenin. **Video 3** is a time-lapse confocal fluorescence video showing the spreading of an  $\alpha$ -catenin KD MEF expressing mCherry-vinculin and WT GFP- $\alpha$ -catenin. **Video 4** is a time-lapse confocal fluorescence video showing the spreading of an  $\alpha$ -catenin KD MEF expressing mCherry-vinculin and GFP- $\alpha$ -catenin-L344P. **Video 5** is a time-lapse bright-field video of an  $\alpha$ -catenin KD MEF during early stages of cell spreading. **Video 6** is a time-lapse bright-field video of an  $\alpha$ -catenin KD MEF expressing GFP- $\alpha$ -catenin-L344P during early stages of cell spreading. **Video 7** is a time-lapse bright-field video of a WT MEF

during early stages of cell spreading. **Video 8** is a time-lapse bright-field video of an  $\alpha$ -catenin KD MEF expressing WT GFP- $\alpha$ -catenin during early stages of cell spreading. **Video 9** is a time-lapse confocal fluorescence video showing a protrusion of an  $\alpha$ -catenin KD MEF expressing mCherry-vinculin and GFP- $\alpha$ -catenin-L344P. **Video 10** is a time-lapse confocal fluorescence video showing the spreading of an  $\alpha$ -catenin KD MEF expressing tdTomato-Tractin and GFP- $\alpha$ -catenin-L344P.

### Acknowledgments

H. Wolfenson acknowledges support from the Israel Science Foundation (1738/17) and from the Rappaport Family Foundation. H. Wolfenson is an incumbent of the David and Inez Myers Career Advancement Chair in Life Sciences.

The authors declare no competing financial interests.

Author contributions: A. Mukherjee performed most of the experiments and data analyses; S. Melamed performed the co-IP experiments; H. Damouny-Khoury assisted with the Western blots; M. Amer performed the real-time PCR; L. Feld assisted with the immunostaining; E. Nadjar-Boger performed cloning and assisted in generation of KD cell lines; M.P. Sheetz and H. Wolfenson conceived the idea for the studies. H. Wolfenson supervised the studies. A. Mukherjee and H. Wolfenson wrote the manuscript.

Submitted: 22 February 2021

Revised: 22 December 2021

Accepted: 16 May 2022

### References

- Amer, M., L. Shi, and H. Wolfenson. 2021. The “Yin and Yang” of cancer cell growth and mechanosensing. *Cancers*. 13:4754. <https://doi.org/10.3390/cancers13194754>
- Bajpai, S., Y. Feng, R. Krishnamurthy, G.D. Longmore, and D. Wirtz. 2009. Loss of  $\alpha$ -catenin decreases the strength of single E-cadherin bonds between human cancer cells. *J. Biol. Chem.* 284:18252–18259. <https://doi.org/10.1074/jbc.M109.000661>
- Barry, A.K., H. Tabdili, I. Muhamed, J. Wu, N. Shashikanth, G.A. Gomez, A.S. Yap, C.J. Gottardi, J. De Rooij, N. Wang, and D.E. Leckband. 2014.  $\alpha$ -Catenin cytomechanics: Role in cadherin-dependent adhesion and

- mechanotransduction. *J. Cell Sci.* 127:1779–1791. <https://doi.org/10.1242/jcs.139014>
- Belin, B.J., L.M. Goins, and R.D. Mullins. 2014. Comparative analysis of tools for live cell imaging of actin network architecture. *Bioarchitecture*. 4: 189–202. <https://doi.org/10.1080/19490992.2014.1047714>
- Benjamin, J.M., A.V. Kwiatkowski, C. Yang, F. Korobova, S. Pokutta, T. Svitkina, W.I. Weis, and W.J. Nelson. 2010.  $\alpha$ E-catenin regulates actin dynamics independently of cadherin-mediated cell–cell adhesion. *J. Cell Biol.* 189:339–352. <https://doi.org/10.1083/jcb.200910041>
- Buckley, C.D., J. Tan, K.L. Anderson, D. Hanein, N. Volkmann, W.I. Weis, W.J. Nelson, and A.R. Dunn. 2014. Cell adhesion. The minimal cadherin–catenin complex binds to actin filaments under force. *Science*. 346: 1254211. <https://doi.org/10.1126/science.1254211>
- Changede, R., X. Xu, F. Margadant, and M.P. Sheetz. 2015. Nascent integrin adhesions form on all matrix rigidities after integrin activation. *Dev. Cell*. 35:614–621. <https://doi.org/10.1016/j.devcel.2015.11.001>
- Chorev, D.S., O. Moscovitz, B. Geiger, and M. Sharon. 2014. Regulation of focal adhesion formation by a vinculin–Arp2/3 hybrid complex. *Nat. Commun.* 5:3758. <https://doi.org/10.1038/ncomms4758>
- Cohen, D.M., B. Kutscher, H. Chen, D.B. Murphy, and S.W. Craig. 2006. A conformational switch in vinculin drives formation and dynamics of a talin–vinculin complex at focal adhesions. *J. Biol. Chem.* 281: 16006–16015. <https://doi.org/10.1074/jbc.M600738200>
- Driscoll, T.P., S.J. Ahn, B. Huang, A. Kumar, and M.A. Schwartz. 2020. Actin flow-dependent and -independent force transmission through integrins. *Proc. Natl. Acad. Sci. USA*. 117:32413–32422. <https://doi.org/10.1073/pnas.2010292117>
- Edelstein, A., N. Amodaj, K. Hoover, R. Vale, and N. Stuurman. 2010. Computer control of microscopes using  $\mu$ Manager. *Curr. Protoc. Mol. Biol.* Chapter 14:Unit14.20. <https://doi.org/10.1002/0471142727.mb1420s92>
- Elosegui-Artola, A., R. Oria, Y. Chen, A. Kosmalska, C. Perez-Gonzalez, N. Castro, C. Zhu, X. Trepast, and P. Roca-Cusachs. 2016. Mechanical regulation of a molecular clutch defines force transmission and transduction in response to matrix rigidity. *Nat. Cell Biol.* 18:540–548. <https://doi.org/10.1038/ncb3336>
- Feld, L., L. Kellerman, A. Mukherjee, A. Livne, E. Bouchbinder, and H. Wolfenson. 2020. Cellular contractile forces are nonmechanosensitive. *Sci. Adv.* 6:eaa6997. <https://doi.org/10.1126/SCIADV.AAZ6997>
- Galbraith, C.G., K.M. Yamada, and M.P. Sheetz. 2002. The relationship between force and focal complex development. *J. Cell Biol.* 159:695–705. <https://doi.org/10.1083/jcb.200204153>
- Ghassemi, S., G. Meacci, S. Liu, A.A. Gondarenko, A. Mathur, P. Roca-Cusachs, M.P. Sheetz, and J. Hone. 2012. Cells test substrate rigidity by local contractions on submicrometer pillars. *Proc. Natl. Acad. Sci. USA*. 109:5328–5333. <https://doi.org/10.1073/pnas.1119886109>
- Guadamillas, M.C., A. Cerezo, and M.A. Del Pozo. 2011. Overcoming anoikis–pathways to anchorage-independent growth in cancer. *J. Cell Sci.* 124:3189–3197. <https://doi.org/10.1242/jcs.072165>
- Hirata, H., H. Tatsumi, C.T. Lim, and M. Sokabe. 2014. Force-dependent vinculin binding to talin in live cells: A crucial step in anchoring the actin cytoskeleton to focal adhesions. *Am. J. Physiol. Cell Physiol.* 306: C607–C620. <https://doi.org/10.1152/ajpcell.00122.2013>
- Ishiyama, N., N. Tanaka, K. Abe, Y.J. Yang, Y.M. Abbas, M. Umitsu, B. Nagar, S.A. Bueler, J.L. Rubinstein, M. Takeichi, et al. 2013. An autoinhibited structure of  $\alpha$ -catenin and its implications for vinculin recruitment to adherens junctions. *J. Biol. Chem.* 288:15913–15925. <https://doi.org/10.1074/jbc.M113.453928>
- Ishiyama, N., R. Sarpal, M.N. Wood, S.K. Barrick, T. Nishikawa, H. Hayashi, A.B. Kobb, A.S. Flozak, A. Yemelyanov, R. Fernandez-Gonzalez, et al. 2018. Force-dependent allostery of the  $\alpha$ -catenin actin-binding domain controls adherens junction dynamics and functions. *Nat. Commun.* 9: 5121. <https://doi.org/10.1038/s41467-018-07481-7>
- Iskratsch, T., H. Wolfenson, and M.P. Sheetz. 2014. Appreciating force and shape—the rise of mechanotransduction in cell biology. *Nat. Rev. Mol. Cell Biol.* 15:825–833. <https://doi.org/10.1038/nrm3903>
- Kobiak, A., and E. Fuchs. 2004.  $\alpha$ -Catenin: At the junction of intercellular adhesion and actin dynamics. *Nat. Rev. Mol. Cell Biol.* 5:614–625. <https://doi.org/10.1038/nrm1433>
- Lu, J., A.D. Doyle, Y. Shinsato, S. Wang, M.A. Bodendorfer, M. Zheng, and K.M. Yamada. 2020. Basement membrane regulates fibronectin organization using sliding focal adhesions driven by a contractile winch. *Dev. Cell*. 52:631–646.e4. <https://doi.org/10.1016/j.devcel.2020.01.007>
- Maiden, S.L., and J. Hardin. 2011. The secret life of  $\alpha$ -catenin: Moonlighting in morphogenesis. *J. Cell Biol.* 195:543–552. <https://doi.org/10.1083/jcb.201103106>
- Meacci, G., H. Wolfenson, S. Liu, M.R. Stachowiak, T. Iskratsch, A. Mathur, S. Ghassemi, N. Gauthier, E. Tabdanov, J. Lohner, et al. 2016.  $\alpha$ -Actinin links extracellular matrix rigidity-sensing contractile units with peridolic cell-edge retractions. *Mol. Biol. Cell*. 27:3471–3479. <https://doi.org/10.1091/mbc.E16-02-0107>
- Nicholl, I.D., T. Matsui, T.M. Weiss, C.B. Stanley, W.T. Heller, A. Martel, B. Farago, D.J.E. Callaway, and Z. Bu. 2018.  $\alpha$ -Catenin structure and nanoscale dynamics in solution and in complex with F-actin. *Biophys. J.* 115:642–654. <https://doi.org/10.1016/j.bpj.2018.07.005>
- Ou, G., D. Thakar, J.C. Tung, Y.A. Miroshnikova, C.C. Dufort, E. Gutierrez, A. Groisman, and V.M. Weaver. 2016. Visualizing mechanical modulation of nanoscale organization of cell–matrix adhesions. *Integr. Biol.* 8: 795–804. <https://doi.org/10.1039/c6ib00031b>
- Parsons, J.T., A.R. Horwitz, and M.A. Schwartz. 2010. Cell adhesion: Integrating cytoskeletal dynamics and cellular tension. *Nat. Reviews. Mol. Cell Biol.* 11:633–643. <https://doi.org/10.1038/nrm2957>
- Peng, X., J.L. Maiers, D. Choudhury, S.W. Craig, and K.A. DeMali. 2012.  $\alpha$ -Catenin uses a novel mechanism to activate vinculin. *J. Biol. Chem.* 287:7728–7737. <https://doi.org/10.1074/jbc.M111.297481>
- Piao, H.L., Y. Yuan, M. Wang, Y. Sun, H. Liang, and L. Ma. 2014.  $\alpha$ -Catenin acts as a tumour suppressor in E-cadherin-negative basal-like breast cancer by inhibiting NF- $\kappa$ B signalling. *Nat. Cell Biol.* 16:245–254. <https://doi.org/10.1038/ncb2909>
- Pokutta, S., and W.I. Weis. 2007. Structure and mechanism of cadherins and catenins in cell–cell contacts. *Annu. Rev. Cell Dev. Biol.* 23:237–261. <https://doi.org/10.1146/annurev.cellbio.22.010305.104241>
- Ringer, P., G. Colo, R. Fässler, and C. Grashoff. 2017. Sensing the mechanochemical properties of the extracellular matrix. *Matrix Biol.* 64:6–16. <https://doi.org/10.1016/j.matbio.2017.03.004>
- del Rio, A., R. Perez-Jimenez, R. Liu, P. Roca-Cusachs, J.M. Fernandez, and M.P. Sheetz. 2009. Stretching single talin rod molecules activates vinculin binding. *Science*. 323:638–641. <https://doi.org/10.1126/science.1162912>
- Riveline, D., E. Zamir, N.Q. Balaban, U.S. Schwarz, T. Ishizaki, S. Narumiya, Z. Kam, B. Geiger, and A.D. Bershadsky. 2001. Focal contacts as mechanosensors: Externally applied local mechanical force induces growth of focal contacts by an mDial-dependent and ROCK-independent mechanism. *J. Cell Biol.* 153:1175–1186. <https://doi.org/10.1083/jcb.153.6.1175>
- Roca-Cusachs, P., A. del Rio, E. Puklin-Faucher, N.C. Gauthier, N. Biais, and M.P. Sheetz. 2013. Integrin-dependent force transmission to the extracellular matrix by  $\alpha$ -actinin triggers adhesion maturation. *Proc. Natl. Acad. Sci. USA* 110:E1361–E1370. <https://doi.org/10.1073/pnas.1220723110>
- Sarpal, R., V. Yan, L. Kazakova, L. Sheppard, J.C. Yu, R. Fernandez-Gonzalez, and U. Tepass. 2019. Role of  $\alpha$ -catenin and its mechanosensing properties in regulating Hippo/YAP-dependent tissue growth. *PLoS Genet.* 15:e1008454. <https://doi.org/10.1371/journal.pgen.1008454>
- Seddiki, R., G.H.N.S. Narayana, P.-O. Strale, H.E. Balcioglu, G. Peyret, M. Yao, A.P. Le, C. Teck Lim, J. Yan, B. Ladoux, and R.M. Mège. 2018. Force-dependent binding of vinculin to  $\alpha$ -catenin regulates cell–cell contact stability and collective cell behavior. *Mol. Biology Cell*. 29:380–388. <https://doi.org/10.1091/mbc.E17-04-0231>
- Silvis, M.R., B.T. Kreger, W.H. Lien, O. Klezovitch, G.M. Rudakova, F.D. Camargo, D.M. Lantz, J.T. Seykora, and V. Vasioukhin. 2011.  $\alpha$ -Catenin is a tumor suppressor that controls cell accumulation by regulating the localization and activity of the transcriptional coactivator yap1. *Sci. Signal.* 4:ra33. <https://doi.org/10.1126/scisignal.2001823>
- Su, J., M. Muranjan, and J. Sap. 1999. Receptor protein tyrosine phosphatase alpha activates Src-family kinases and controls integrin-mediated responses in fibroblasts. *Curr. Biol.* 9:505–511. [https://doi.org/10.1016/s0960-9822\(99\)80234-6](https://doi.org/10.1016/s0960-9822(99)80234-6)
- Sun, Y., J. Zhang, and L. Ma. 2014.  $\alpha$ -Catenin. A tumor suppressor beyond adherens junctions. *Cell Cycle*. 13:2334–2339. <https://doi.org/10.4161/cc.29765>
- Thomas, W.A., C. Boscher, Y.S. Chu, D. Cuvelier, C. Martinez-Rico, R. Seddiki, J. Heysch, B. Ladoux, J.P. Thiery, R.M. Mege, and S. Dufour. 2013.  $\alpha$ -Catenin and vinculin cooperate to promote high E-cadherin-based adhesion strength. *J. Biol. Chem.* 288:4957–4969. <https://doi.org/10.1074/jbc.M112.403774>
- Vassilev, V., A. Platek, S. Hiver, H. Enomoto, and M. Takeichi. 2017. Catenins steer cell migration via stabilization of front–rear polarity. *Dev. Cell*. 43: 463–479.e5. <https://doi.org/10.1016/j.devcel.2017.10.014>
- Wei, S.C., L. Fattet, J.H. Tsai, Y. Guo, V.H. Pai, H.E. Majeski, A.C. Chen, R.L. Sah, S.S. Taylor, A.J. Engler, and J. Yang. 2015. Matrix stiffness drives

- epithelial-mesenchymal transition and tumour metastasis through a TWIST1-G3BP2 mechanotransduction pathway. *Nat. Cell Biol.* 17: 678–688. <https://doi.org/10.1038/ncb3157>
- Wolfenson, H., I. Lavelin, and B. Geiger. 2013. Dynamic regulation of the structure and functions of integrin adhesions. *Dev. Cell.* 24:447–458. <https://doi.org/10.1016/j.devcel.2013.02.012>
- Wolfenson, H., G. Meacci, S. Liu, M.R. Stachowiak, T. Iskratsch, S. Ghassemi, P. Roca-Cusachs, B. O’Shaughnessy, J. Hone, and M.P. Sheetz. 2016. Tropomyosin controls sarcomere-like contractions for rigidity sensing and suppressing growth on soft matrices. *Nat. Cell Biol.* 18:33–42. <https://doi.org/10.1038/ncb3277>
- Wood, M.N., N. Ishiyama, I. Singaram, C.M. Chung, A.S. Flozak, A. Yemelyanov, M. Ikura, W. Cho, and C.J. Gottardi. 2017.  $\alpha$ -Catenin homodimers are recruited to phosphoinositide-activated membranes to promote adhesion. *J. Cell Biol.* 216:3767–3783. <https://doi.org/10.1083/jcb.201612006>
- Xu, W., H. Baribault, and E.D. Adamson. 1998. Vinculin knockout results in heart and brain defects during embryonic development. *Development.* 125:327–337. <https://doi.org/10.1242/dev.125.2.327>
- Yang, B., H. Wolfenson, V.Y. Chung, N. Nakazawa, S. Liu, J. Hu, R.Y.-J. Huang, and M.P. Sheetz. 2020. Stopping transformed cancer cell growth by rigidity sensing. *Nat. Mater.* 19:239–250. <https://doi.org/10.1038/s41563-019-0507-0>
- Yap, A.S., K. Duszyc, and V. Viasnoff. 2018. Mechanosensing and mechanotransduction at cell–cell junctions. *Cold Spring Harbor Perspect. Biol.* 10: a028761. <https://doi.org/10.1101/cshperspect.a028761>
- Yonemura, S., Y. Wada, T. Watanabe, A. Nagafuchi, and M. Shibata. 2010.  $\alpha$ -Catenin as a tension transducer that induces adherens junction development. *Nat. Cell Biol.* 12:533–542. <https://doi.org/10.1038/ncb2055>
- Zaidel-Bar, R., C. Ballestrem, Z. Kam, and B. Geiger. 2003. Early molecular events in the assembly of matrix adhesions at the leading edge of migrating cells. *J. Cell Sci.* 116:4605–4613. <https://doi.org/10.1242/jcs.00792>
- Zhang, Y.-H., C.-Q. Zhao, L.-S. Jiang, and L.-Y. Dai. 2011. Substrate stiffness regulates apoptosis and the mRNA expression of extracellular matrix regulatory genes in the rat annular cells. *Matrix Biol.* 30:135–144. <https://doi.org/10.1016/j.matbio.2010.10.008>

## Supplemental material

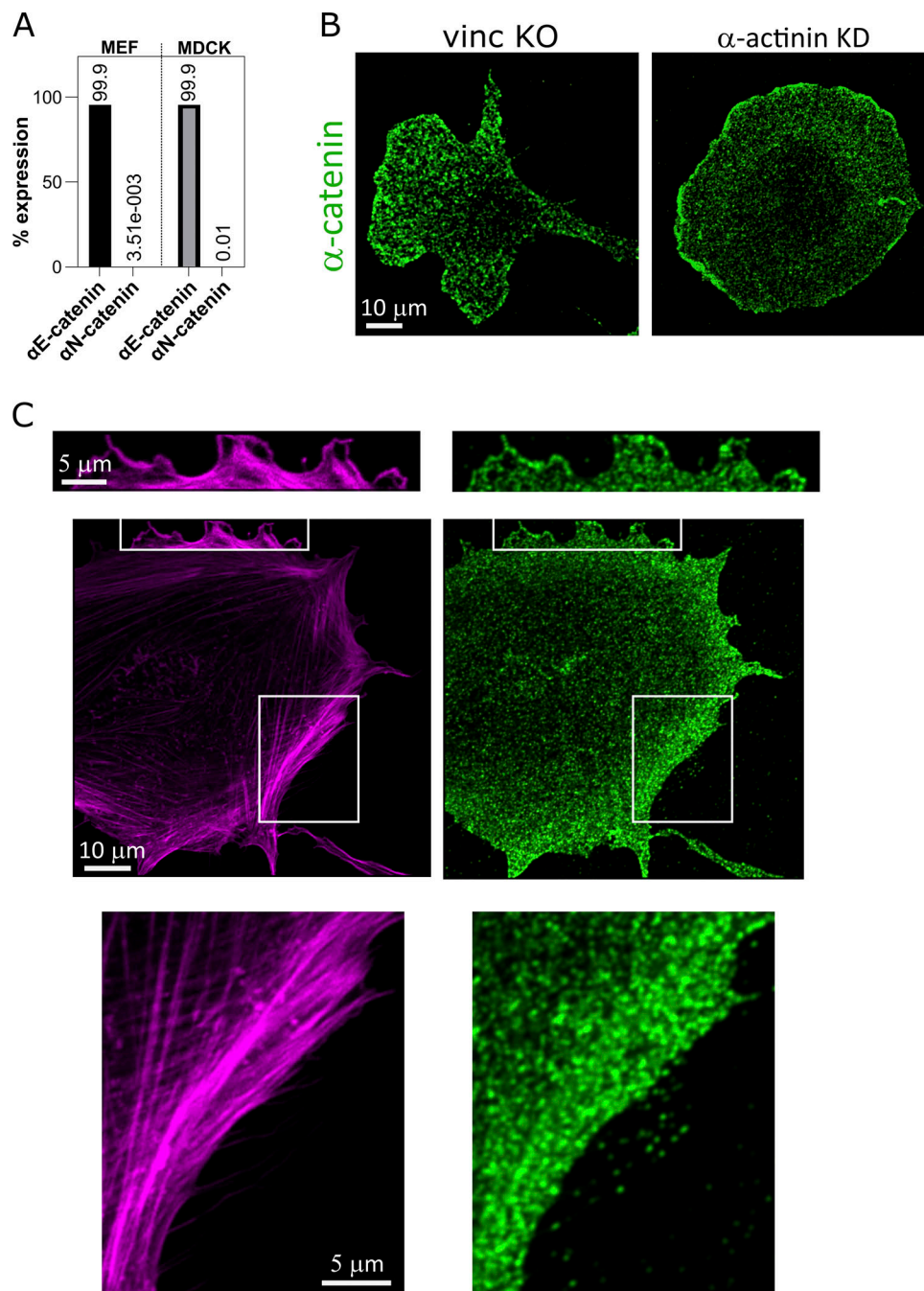


Figure S1. **α-Catenin colocalizes with F-actin.** (A) RT-PCR analyses show that MEF and MDCK cells (used later in this study, see Fig. 5) express almost exclusively αE-catenin and not αN-catenin. (B) Immunostaining for α-catenin in vinculin<sup>-/-</sup> cells and α-actinin KD MEFs shows that its recruitment to the cell edge is not impaired by the absence of either of these proteins. (C) Immunostaining for α-catenin (green) in MEFs fixed 4 h after plating on FN-coated glass shows colocalization with F-actin (magenta) on stress fibers (bottom zoom-in) as well as at the cell edge (top zoom-in). The brightness of the top rectangle in the zoomed-out image was enhanced for the purpose of clarity.

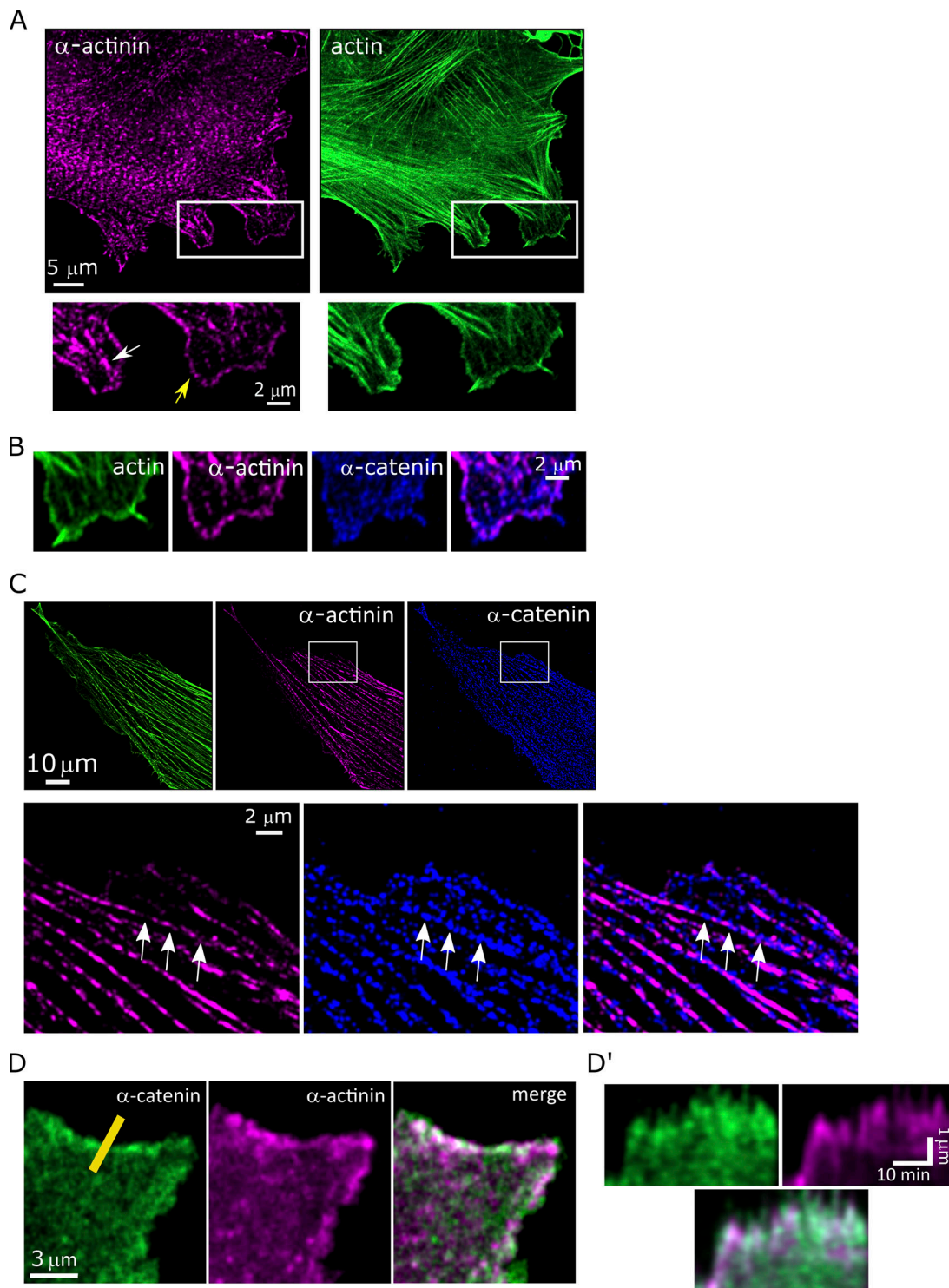


Figure S2.  **$\alpha$ -Catenin and  $\alpha$ -actinin do not colocalize.** (A) Immunostaining in WT MEFs for  $\alpha$ -actinin shows its colocalization after 15 min of spreading with F-actin at the cell edge (yellow arrow) as well as its localization in nascent adhesions (white arrow). (B) Zoom-in on the edge of a WT MEF cell costained for actin,  $\alpha$ -actinin,  $\alpha$ -catenin, showing lack of overlap of the latter two. (C) Immunostaining for  $\alpha$ -actinin and  $\alpha$ -catenin in WT MEFs shows their lack of overlap in actin stress fibers. Bottom row is the zoom-in of the boxes in the top row; arrows point to locations in which  $\alpha$ -catenin is localized but  $\alpha$ -actinin is not. (D) Frame from a video of a cell expressing GFP- $\alpha$ -catenin and mCherry- $\alpha$ -actinin showing that the two are not colocalized; and kymographs taken from the yellow line (D').

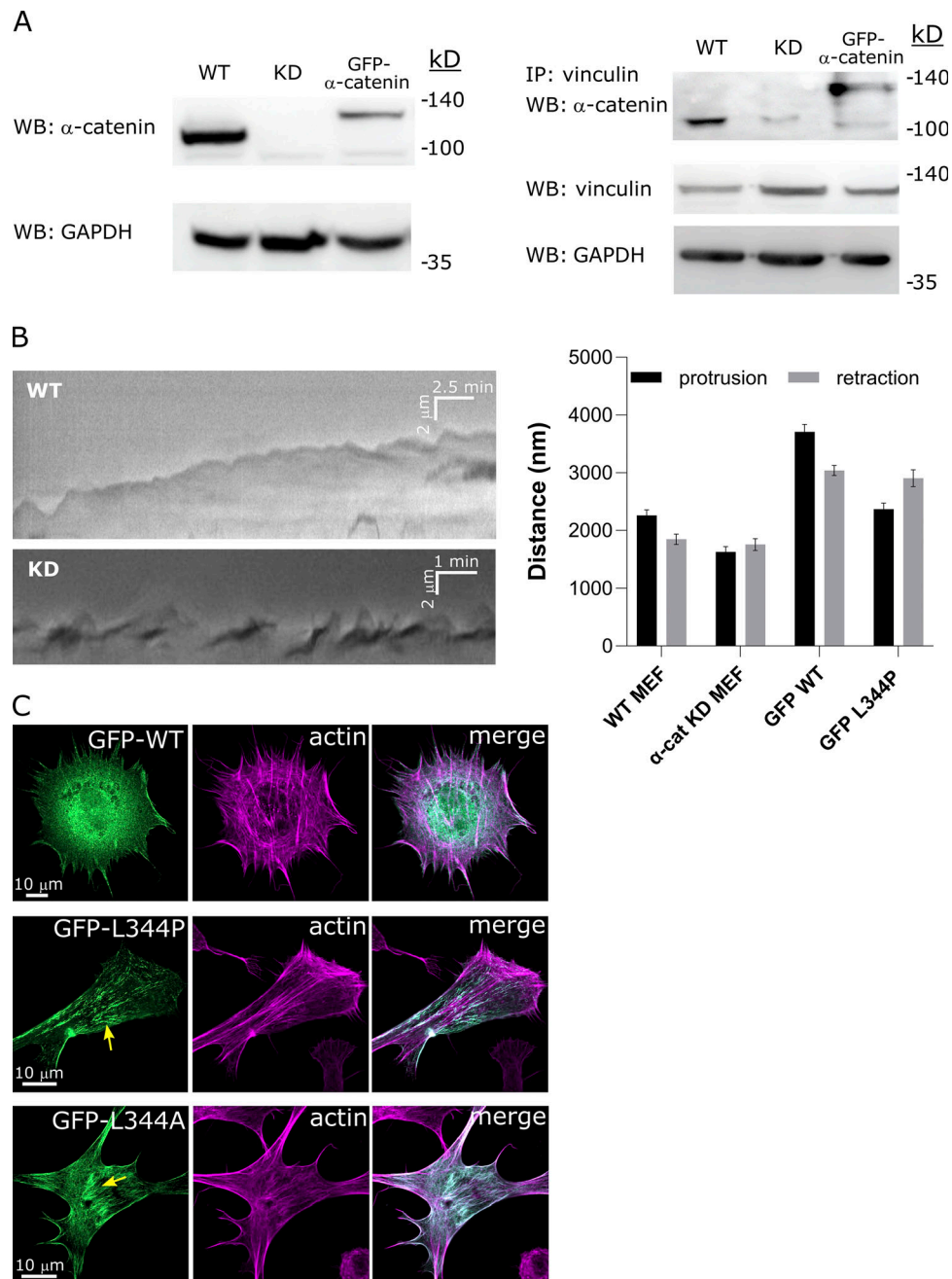


Figure S3.  **$\alpha$ -Catenin regulates cell edge protrusion-retraction cycles and cytoskeletal organization.** (A) Left: Immunoblot for  $\alpha$ -catenin in lysates taken from WT MEFs,  $\alpha$ -catenin KD MEFs, and  $\alpha$ -catenin KD MEFs expressing WT GFP- $\alpha$ -catenin. Right: Immunoprecipitation for vinculin followed by immunoblot for  $\alpha$ -catenin; below is a blot for vinculin from the cell lysates. WB, Western blot. (B) Left: Kymographs of the cell edge taken from time-lapse videos of early spreading by WT and  $\alpha$ -catenin KD MEFs showing regular protrusion-retraction cycles in the former and extensive ruffling in the latter. Right: quantifications of the distances traveled during the protrusion and retraction phases by WT MEFs,  $\alpha$ -catenin KD MEFs,  $\alpha$ -catenin KD MEFs expressing WT GFP- $\alpha$ -catenin, and  $\alpha$ -catenin KD MEFs expressing GFP- $\alpha$ -catenin L344P. WT and GFP-WT cells display longer protrusions than retractions, whereas KD and L344P cells do not, consistent with ruffling.  $n > 30$  cycles from at least eight cells in each case. (C) F-actin staining (phalloidin) in vinculin<sup>-/-</sup> MEF cells expressing WT GFP- $\alpha$ -catenin, GFP- $\alpha$ -catenin L344P, and GFP- $\alpha$ -catenin L344A. The yellow arrows point to actin aggregates near the cell center. Source data are available for this figure: SourceData FS3.

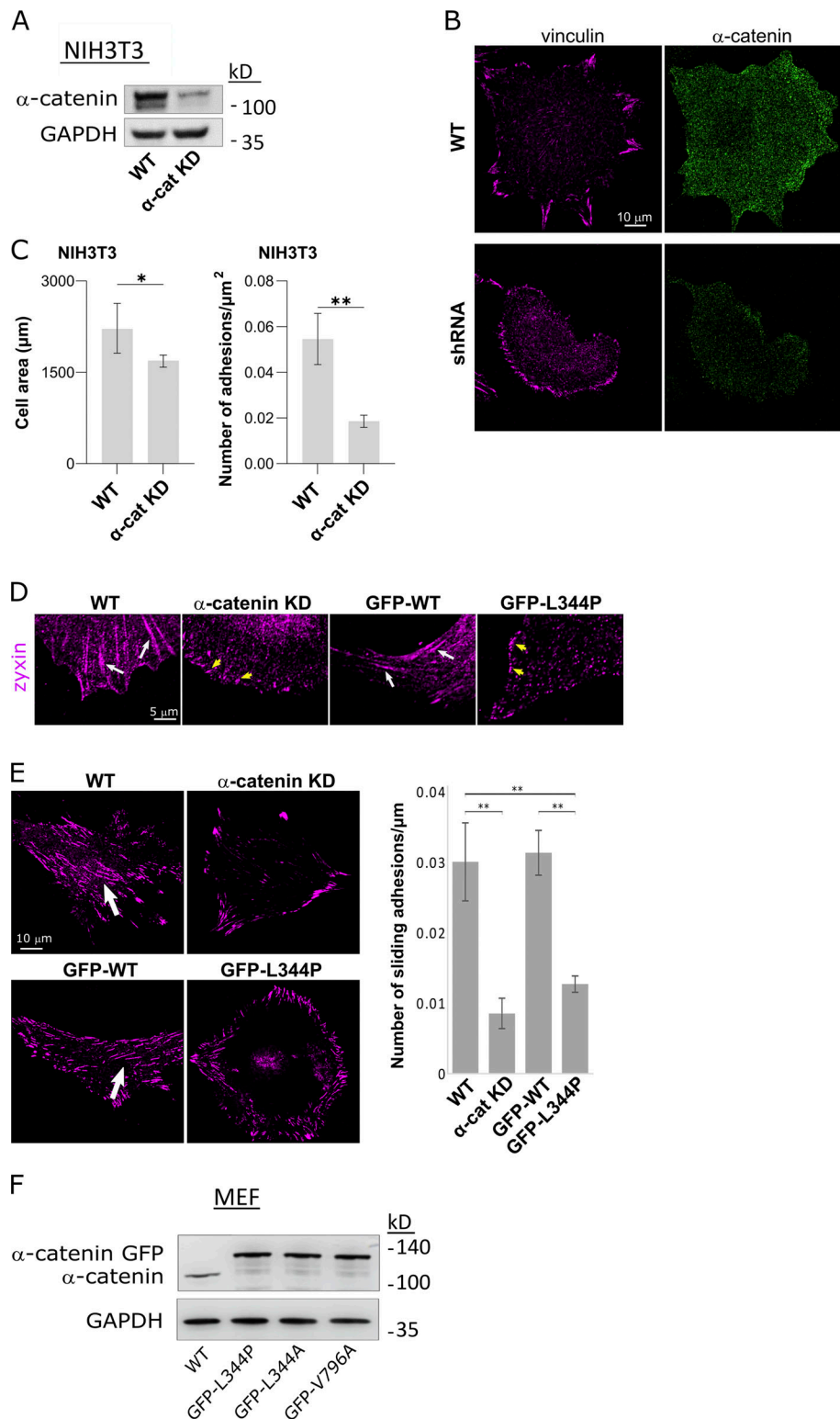


Figure S4. **α-Catenin regulates adhesion maturation.** (A) Immunoblot for α-catenin showing KD in NIH3T3 cells. (B) Immunostaining for vinculin and α-catenin in WT and α-catenin KD NIH3T3 cells. (C) Quantification of cell area and number of mature adhesions per square micrometer in WT and α-catenin KD NIH3T3 cells.  $n = 17$  cells in each case. (D) Immunostaining for zyxin shows the presence of mature adhesions in WT MEFs and α-catenin KD cells expressing WT GFP-α-catenin (white arrows), but only the presence of focal complexes in α-catenin KD cells and α-catenin KD cells expressing GFP-α-catenin L344P (yellow arrows). (E) Formation of sliding adhesions (arrows) on Matrigel-coated coverslips by WT cells, α-catenin KD cells, and α-catenin KD cells expressing WT GFP-α-catenin or GFP-α-catenin L344P ( $n > 15$  cells in each case). (F) Immunoblot for α-catenin in WT MEFs and α-catenin KD cells expressing GFP-α-catenin L344P, GFP-α-catenin L344A, and GFP-α-catenin V796A. Statistical analysis for the NIH3T3 cell area and number of adhesions was performed with two-tailed unpaired *t* test followed by Welch's correction. Statistical analysis of the number of sliding adhesions was performed by ANOVA followed by Tukey's post hoc test correction (\*,  $P < 0.05$ ; \*\*,  $P < 0.01$ ). Source data are available for this figure: SourceData FS4.

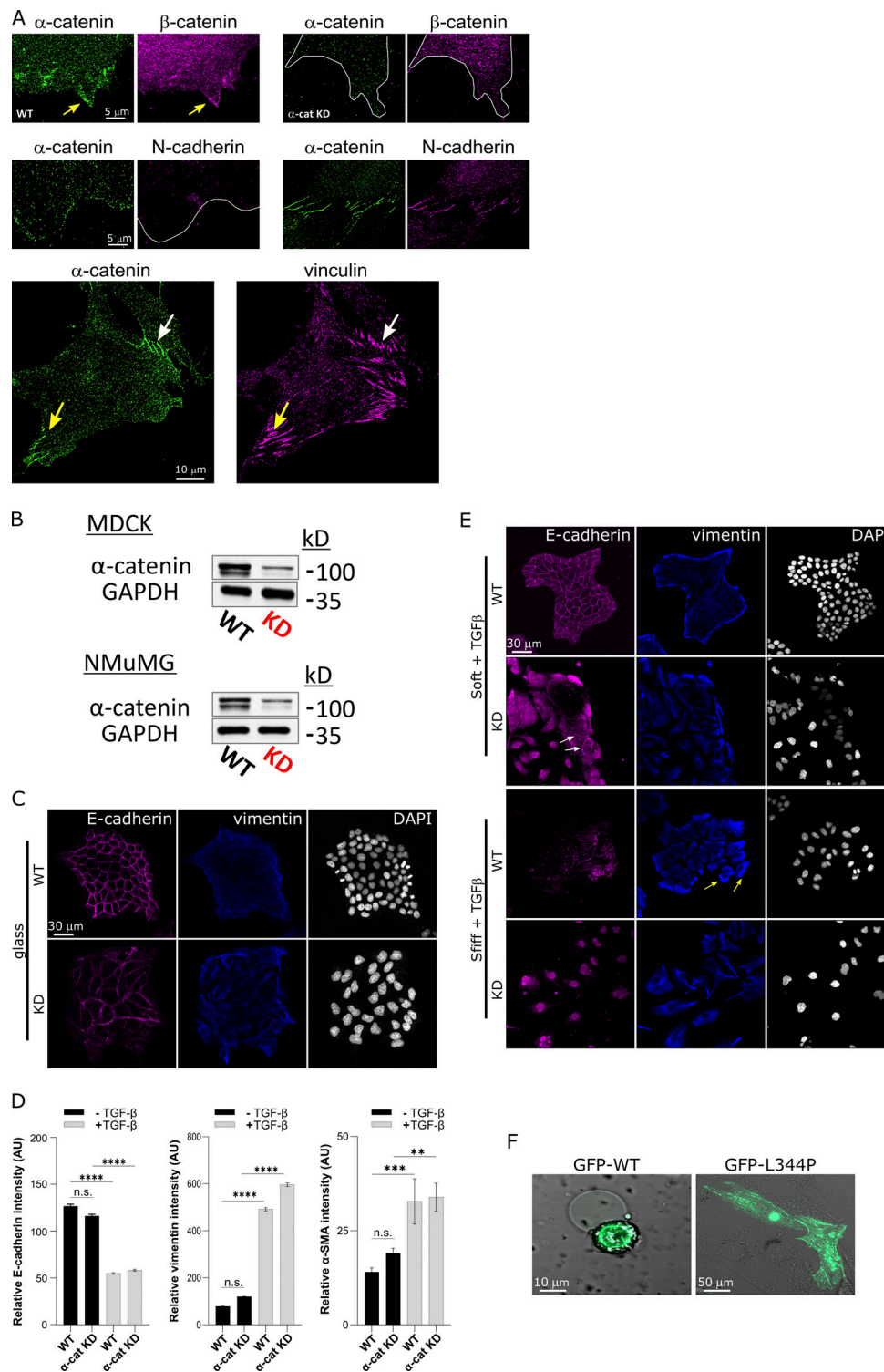


Figure S5.  **$\alpha$ -Catenin plays a role in TGF- $\beta$ -induced EMT.** (A) Top:  $\alpha$ -Catenin and  $\beta$ -catenin localize at the cell edge, but  $\beta$ -catenin is missing from the edge upon  $\alpha$ -catenin KD. Middle: N-cadherin is localized in cell-cell junctions (right) but not at the cell edge (left) in WT MEFs. Bottom: Mature FAs (yellow arrow) form in extensions rich with  $\alpha$ -catenin in cells that also form  $\alpha$ -catenin-rich cell-cell contacts (white arrow). (B) Immunoblot for  $\alpha$ -catenin showing KD in MDCK and NMuMG cells. (C) WT and  $\alpha$ -catenin KD MDCK cells stained for E-cadherin and vimentin after 48 h on FN-coated glass without stimulation for EMT. (D) Quantifications of E-cadherin, vimentin, and  $\alpha$ -SMA intensity in WT and KD cells untreated or after 72 h treatment with TGF $\beta$ . (E) WT and  $\alpha$ -catenin KD MDCK cells stained for E-cadherin and vimentin after 72 h incubation with TGF $\beta$  (10 ng/ml) on FN-coated soft (0.2-kPa) and stiff (25-kPa) matrices.  $n > 22$  cells in each case. (F)  $\alpha$ -catenin KD MEFs expressing WT GFP- $\alpha$ -catenin or GFP- $\alpha$ -catenin L344P, plated for 24 h on 0.2-kPa FN-coated matrices. The L344P mutant localizes to actin bundles in central regions of the cells (similar to Fig. 3, C and E). Statistical analysis comparing the relative intensities of the EMT markers was performed by ANOVA followed by Tukey's post hoc test correction (\*\*,  $P < 0.01$ ; \*\*\*,  $P < 0.001$ ; \*\*\*\*,  $P < 0.0001$ ). Source data are available for this figure: SourceData FS5.

Video 1. **Time-lapse confocal fluorescence microscopy of an  $\alpha$ -catenin KD MEF expressing tdTomato-Tractin (magenta) and WT GFP- $\alpha$ -catenin (green).** Images were acquired every 30 s for 120 min. Playback, 30 fps.

Video 2. **Time-lapse confocal fluorescence microscopy of an  $\alpha$ -catenin KD MEF expressing mCherry- $\alpha$ -actinin (magenta) and WT GFP- $\alpha$ -catenin (green).** Images were acquired every 30 s for 36.5 min. Playback, 20 fps.

Video 3. **Time-lapse confocal fluorescence microscopy of an  $\alpha$ -catenin KD MEF expressing mCherry-vinculin (magenta) and WT GFP- $\alpha$ -catenin (green).** Images were acquired every 20 s for 120 min. Playback, 20 fps. The white arrows follow maturing FAs.

Video 4. **Time-lapse confocal fluorescence microscopy of an  $\alpha$ -catenin KD MEF expressing mCherry-vinculin (magenta) and GFP- $\alpha$ -catenin-L344P (green).** Images were acquired every 20 s for 77 min. Playback, 20 fps.

Video 5. **Time-lapse bright-field microscopy of an  $\alpha$ -catenin KD MEF during early stages of cell spreading.** Images were acquired every 2 s for 15 min. Playback, 50 fps.

Video 6. **Time-lapse bright-field microscopy of an  $\alpha$ -catenin KD MEF expressing GFP- $\alpha$ -catenin-L344P (fluorescent channel not shown) during early stages of cell spreading.** Images were acquired every 2 s for 15 min. Playback, 50 fps.

Video 7. **Time-lapse bright-field microscopy of a WT MEF during early stages of cell spreading.** Images were acquired every 2 s for 15 min. Playback, 50 fps.

Video 8. **Time-lapse bright-field microscopy of an  $\alpha$ -catenin KD MEF expressing WT GFP- $\alpha$ -catenin (fluorescent channel not shown) during early stages of cell spreading.** Images were acquired every 2 s for 15 min. Playback, 50 fps.

Video 9. **Time-lapse confocal fluorescence microscopy of a protrusion of an  $\alpha$ -catenin KD MEF expressing mCherry-vinculin (magenta) and GFP- $\alpha$ -catenin-L344P (green).** Images were acquired every 20 s for 60 min. Playback, 20 fps.

Video 10. **Time-lapse confocal fluorescence microscopy of an  $\alpha$ -catenin KD MEF expressing tdTomato-Tractin (magenta) and GFP- $\alpha$ -catenin-L344P (green).** Images were acquired every 30 s for 66 min. Playback, 25 fps.